HHS Public Access

Author manuscript

Free Radic Biol Med. Author manuscript; available in PMC 2023 March 24.

Published in final edited form as:

Free Radic Biol Med. 2019 March ; 133: 295–309. doi:10.1016/j.freeradbiomed.2018.12.013.

Suppressive effects of iron chelation in clear cell renal cell carcinoma and their dependency on VHL inactivation

Christopher J. Greene[1], **Nitika J. Sharma**[1], **Peter N. Fiorica**[1], **Emily Forrester**[1], **Gary J. Smith**[1], **Kenneth W. Gross**[2], **Eric C. Kauffman**[1,3,4]

[1]Department of Urology, Roswell Park Comprehensive Cancer Center, Buffalo, NY 14263

[2]Department of Molecular and Cellular Biology, Roswell Park Comprehensive Cancer Center, Buffalo, NY 14263

[3]Department of Cancer Genetics, Roswell Park Comprehensive Cancer Center, Buffalo, NY 14263

[4]Jacobs School of Medicine and Biomedical Sciences, State University of New York at Buffalo, Buffalo, NY 14214

Abstract

Background and Objectives: Accumulating data implicate iron accumulation in tumorigenesis of the kidney, particularly the clear cell renal cell carcinoma (ccRCC) subtype. The von Hippel Lindau (VHL)/hypoxia inducible factor-α (HIF-α) axis is uniquely dysregulated in ccRCC and is a major regulator and regulatory target of iron metabolism, yet the role of iron in ccRCC tumorigenesis and its potential interplay with VHL inactivation remains unclear. We investigated whether ccRCC iron accumulation occurs due to increased cell dependency on iron for growth and survival as a result of VHL inactivation.

Materials and Methods: Free iron levels were compared between four VHL-mutant ccRCC cell lines (786–0, A704, 769-P, RCC4) and two benign renal tubule epithelial cell lines (RPTEC, HRCEp) using the Phen Green SK fluorescent iron stain. Intracellular iron deprivation was achieved using two clinical iron chelator drugs, deferasirox (DFX) and deferoxamine (DFO), and chelator effects were measured on cell line growth, cell cycle phase, apoptosis, HIF-1α and HIF-2α protein levels and HIF-α transcriptional activity based on expression of target genes *CA9*,

CORRESPONDING AUTHOR: Eric C. Kauffman, MD , Assistant Professor of Oncology , Departments of Urology and Cancer Genetics , Roswell Park Comprehensive Cancer Center , Elm and Carlton Streets , Buffalo, NY 14263 , Ph: 716-845-3389 , Fax: 716-845-3300 , Eric.kauffman@roswellpark.org.

AUTHOR CONTRIBUTIONS

Manuscript composition was performed by C.J. Greene and E.C. Kauffman, and editorial support was provided by N.J. Sharma, K.W. Gross and G.J. Smith. C.J. Greene and N.J. Sharma were responsible for all experimental techniques and statistical analyses. P. Fiorica assisted with cell culture and gene expression studies. E. Forrester assisted with iron level measurement including assay optimization. K.W. Gross and G.J. Smith provided intellectual and technical support. E.C. Kauffman was responsible for project conception and supervised all members of the research team and all experimental aspects.

CONFLICTS OF INTEREST

The authors declare no conflict of interest.

OCT4/*POU5F1* and *PDGFβ*/*PDGFB*. Similar assays were performed in VHL-mutant ccRCC cells with and without ectopic wild-type VHL expression.

Results: Free iron levels were significantly higher in ccRCC cell lines than benign renal cell lines. DFX depleted cellular free iron more rapidly than DFO and led to greater growth suppression of ccRCC cell lines (>90% at ~30–150 μM) than benign renal cell lines (~10–50% at up to 250 μM). Similar growth responses were observed using DFO, with the exception that a prolonged treatment duration was necessary to deplete cellular iron adequately for differential growth suppression of the less susceptible A704 ccRCC cell line relative to benign renal cell lines. Apoptosis and G1-phase cell cycle arrest were identified as potential mechanisms of chelator growth suppression based on their induction in ccRCC cell lines but not benign renal cell lines. Iron chelation in ccRCC cells but not benign renal cells suppressed HIF-1α and HIF-2α protein levels and transcriptional activity, and the degree and timing of HIF-2α suppression correlated with the onset of apoptosis and differential growth suppression. Restoration of wild-type VHL function in ccRCC cells was sufficient to prevent chelator-induced apoptosis and G1 cell cycle arrest, indicating that ccRCC susceptibility to iron deprivation is VHL inactivation-dependent.

Conclusion: ccRCC cells are characterized by high free iron levels and a cancer-specific dependency on iron for HIF-α overexpression, cell cycle progression and apoptotic escape. This iron dependency is introduced by VHL inactivation, revealing a novel interplay between VHL/HIF-α dysregulation and ccRCC iron metabolism. Future study is warranted to determine if iron deprivation using chelator drugs provides an effective therapeutic strategy for targeting HIF-2α and suppressing tumor progression in ccRCC patients.

Keywords

iron; von Hippel Lindau; hypoxia inducible factor-alpha; clear cell renal cell carcinoma

INTRODUCTION

Iron is the most abundant transition metal in the human body and is involved in a multitude of critical physiologic processes (1–5) due to unique chemical reactivity that enables ready transition between bivalent (ferrous/reduced) and trivalent (ferric/oxidized) states. This feature of iron also drives its classic reaction with hydrogen peroxide to generate potent reactive oxygen species (ROS) (6, 7), namely the hydroxyl radical, which can non-selectively oxidize and damage cellular organic molecules including DNA (8–11). A role for iron in carcinogenesis has long been postulated due to its ability to induce mutagenic DNA breaks and base modifications in addition to epigenetic alterations (8–11). Furthermore, well characterized contributions of iron to DNA replication/cell proliferation, cell cycle progression, mitochondrial metabolism, DNA repair, chromatin remodeling and the cellular stress response (1, 12–26) are speculated to provide a selective advantage to cancers, given the increased need for these processes during tumorigenesis and/or progression.

One cancer in which iron and oxidative stress are well implicated is renal cell carcinoma (RCC) (11, 27–34). RCC accounts for over 90% of kidney cancers and is considered the most lethal genitourinary malignancy (35, 36). RCC is comprised of different histologic subtypes with distinct mutational landscapes and clinical behaviors, and the majority of

RCC diagnoses and deaths are due to the clear cell RCC (ccRCC) subtype (37–40) . ccRCC is unique in that almost all tumors have inactivation of the von Hippel Lindau (*VHL*) gene, which encodes an E3-ubiquitin ligase that cooperates with prolyl hydroxylase (PHD) enzymes to degrade hypoxia-inducible factor-α transcription factors (HIF-1α, HIF-2α) when physiological levels of oxygen and iron are present (38). Normal function of the VHL/PHD/HIF-α axis is inhibited by a reduction in oxygen or iron that promotes HIF-α mediated gene activation and ultimately a return to normoxic cellular conditions (38). *VHL* mutation in 55–75% of ccRCC tumors and promoter hypermethylation in most remaining cases (37, 41–43) leads to HIF-α protein accumulation and upregulation of HIF-α target genes for proliferation, angiogenesis, glycolysis and epithelial-mesenchymal transition (EMT) (38). HIF-2α is likely the critical VHL target for ccRCC tumorigenesis since, unlike HIF-1α, it is overexpressed in 100% of VHL-null ccRCC patient tumors and its overexpression is sufficient to recapitulate the tumorigenic effect of VHL inactivation in ccRCC animal models (43–45). Pharmacologic targeting of HIF-α via indirect approaches (upstream mTOR inhibition, downstream angiogenesis inhibition) is a current standard for advanced ccRCC patient treatment, however clinical responses are nondurable and survival increases are modest (46–48). Thus, there is a critical need to identify additional molecular mechanisms driving HIF-2α-dependent ccRCC tumorigenesis to improve prevention and treatment strategies.

Accumulating evidence from animal models and patient studies suggests a unique role for iron in renal pathophysiology and RCC carcinogenesis. Iron uptake is a master regulatory trigger for embryonic kidney development (49), and we and others have shown that adult renal epithelium expresses among the highest body levels of the primary protein drivers of free (i.e., reactive) iron increases, including transferrin receptor 1 (TFRC/TfR1), divalent metal transporter 1 (SLC11A2/DMT1) and iron regulatory protein 1 (ACO1/IRP1) (28, 50, 51). Although the significance is unclear, this molecular phenotype might predispose renal epithelium to iron overload following episodes of systemic iron elevation (52), as evidenced in patients with acute hemolysis (53). RCC diagnosis risk is increased among individuals with high iron exposure, including iron industry workers and patients with certain chronic anemias that are associated with renal or systemic iron overload; in addition to individuals with a germline miRNA binding site polymorphism in the main iron uptake gene, *TFRC* (29–33, 54). Furthermore, the primary modifiable risk factors for RCC, tobacco and hypertension, increase body iron exposure and trigger renal iron accumulation, respectively (27, 34, 55). Finally, as elegantly characterized by Dr. Toyokuni and others, repeated int raperitoneal administration of chelated ferric iron to rodents causes iron deposition in the proximal renal tubule epithelium (52), the presumed origin of human ccRCC, followed by renal tumorigenesis that mimics human ccRCC in clear cell histology, male gender predominance, and metastatic affinity for lungs and regional lymph nodes (11, 56–61). These tumors are kidney-specific, reproducible across different rat and mouse strains, and have large-scale genomic alterations suggesting molecular similarity to human ccRCC (62).

In addition to these compelling observations, the VHL/HIF-α axis that plays a central role in ccRCC carcinogenesis is both a major regulator and regulatory target of iron metabolism. Gene targets of HIF-α include the major drivers of iron import, *TFRC* and *SLC11A2* (54, 63, 64), and additional interplay between iron and HIF-2α is mediated by

IRP1, which directly modulates translation of iron metabolism gene transcripts harboring a unique iron-responsive element (IRE) motif (65). Intriguingly, a functional IRE motif has been confirmed in the HIF-2α transcript that drives IRP1-dependent HIF-2α translation in response to free iron (66), which suggests that iron deprivation might be an effective strategy for targeting HIF-2α in ccRCC patients. At present, iron deprivation is achieved clinically using iron chelator drugs, including deferoxamine (DFO) and deferasirox (DFX), both of which have demonstrated safety and efficacy in patients with iron overload conditions (67–70). Both drugs also have shown efficacy in various preclinical cancer models, as well as small clinical trials in hepatocellular carcinoma and neuroblastoma patients (71, 72). Presumably these cancers had a functional VHL/PHD/HIF-α axis, and the efficacy of iron chelation in ccRCC with VHL inactivation and HIF-2α hyperactivation has not been previously studied.

The current report investigated the *in vitro* growth suppression efficacy of iron chelation with DFO and DFX in ccRCC cell line models. We hypothesized that ccRCC cells accumulate iron as a result of increased dependency on iron for growth and survival, which is due at least in part to VHL/HIF-α dysregulation. To test this hypothesis, we compared free iron levels and effects of DFO and DFX on growth, cell cycle progression, apoptosis and HIF-α activity in VHL-mutant ccRCC cell lines and benign renal epithelial cell lines. We also examined the interplay between VHL/HIF-α axis dysregulation and free iron levels using VHL-mutant ccRCC cells engineered with restored wild-type VHL function. Our findings reveal the existence of free iron accumulation in ccRCC cells and a cancer-specific dependency on free iron for HIF-α overexpression, cell cycle progression and escape from apoptosis; a dependency that is intriguingly introduced as a result of VHL inactivation. Collectively, this work uncovers a novel cooperative interplay between VHL inactivation and ccRCC iron dependency, and identifies iron chelation as a promising therapeutic strategy for suppressing HIF-2α and ccRCC growth.

MATERIALS AND METHODS

Cell lines and Drugs

Iron chelator drugs were obtained from Selleck Chemicals (Houston, TX) for DFX and from Sigma-Aldrich (St. Louis, MO) for DFO. The 786–0, A704 and 769-P ccRCC cell lines and the HRCEp (Human Renal Cortical Epithelium, also known as HRCE) and RPTEC (Renal Proximal Tubule Epithelial Cell) human benign renal cell lines were obtained from the American Type Culture Collection (Rockville, MD). The RCC4 ccRCC cell line was obtained from the European Collection of Authenticated Cell Cultures General Cell Collection (Salisbury, UK). The 786–0, 769-P, A704 and RCC4 cell lines are derived from ccRCC patient primary renal tumors and harbor known VHL mutations. RCC4 cells stably transfected with the pcDNA3-VHL vector for ectopic expression of wild-type VHL protein (RCC4-VHL) and RCC4 cells stably transfected with the pcDNA3 empty vector (RCC4-EV) were obtained from Sigma Aldrich. All cell lines were cultured *in vitro* in DMEM media supplemented with L-glutamine (4 mM), sodium pyruvate (110mg/L), glucose (4.5g/L) (Corning Cellgro, Manassas, VA), penicillin-streptomycin (100U) (Corning Cellgro) and 10% fetal bovine serum (Thermo Fisher Scientific, Grand Island, NY). RCC4-

EV and RCC4-VHL cell line cultures were additionally supplemented with 0.5 mg/mL G418 selection antibiotic to select for cells harboring the pcDNA3 vector. Cultures were maintained at 37°C with 5% CO2.

Intracellular free iron measurement

Cells were harvested using Trypsin (0.25%, Corning, Tweksbury, MA), washed with Phosphate Buffered Saline (PBS) and incubated in 500 μL Phen Green SK Diacetate (5 μM, Thermo Fisher Scientific, Grand Island, NY) for 30 minutes at 37°C. Stained cells were washed once and resuspended in 200 μL PBS, to which 5 μL of 1:10 diluted Live-Dead Yellow (LDY) stain (Thermo Fisher Scientific) was added. The mixture was incubated for 10 minutes at room temperature in the dark. Sample acquisition was performed using the LSR Fortessa B flow cytometer (BD Biosciences, San Jose, CA) with at least 10,000 events recorded per sample using the Diva software. The Mean Fluorescence Intensity (MFI) of Phen Green staining was calculated for viable cells (LDY negative) using the WinList 9.0.1 software (Verity Software House, Topsham, ME).

Cell line growth assay

ccRCC and benign renal epithelial cells were grown in 96-well plates overnight and treated with different serially diluted concentrations of DFO or DFX for 72 hours or 120 hours. At least triplicate wells were used for each concentration. Cell line growth was assessed using the CellTiter 96® AQueous One Solution Cell Proliferation Assay (MTS) (Promega Life Sciences, Madison, WI) per the manufacturer's instructions. Absorbance at 490 nm was measured using an Xmark microplate reader (Bio-rad, Hercules, CA). Corrected absorbance values were determined by subtracting the mean background absorbance value calculated from cell-free control wells. Growth of treated cells relative to untreated cells was determined as the ratio of their corrected absorbance values.

Annexin V apoptosis assay

Cells were treated with various concentrations of DFO or DFX for 48 hours or 120 hours, or with staurosporine (1 μM) for 18 hours as a positive control for apoptosis. The non-adherent cell fraction was collected from media, while the adhered cell fraction was harvested using trypsin. Cell fractions were re-combined, washed with FACS buffer, re-suspended in 100 μL of assay buffer, and stained for the Annexin V apoptosis marker and 7AAD non-specific cell death marker using the PE Annexin V apoptosis detection kit (Biolegend, San Diego, CA) per manufacturer's instructions. Sample acquisition was performed using a BD FACS Caliber or LSR Fortessa B (BD Biosciences), with at least 10,000 events recorded per sample using Cell Quest or Diva software.

Caspase 3 apoptosis assay

Cells were treated with 125 μM DFO for 48 hours or with 1 μM staurosporine for 18 hours in 96 well plates. Activation of caspase 3 was determined using the Caspase-Glo 3/7 assay (Promega Life Sciences) following the manufacturer's instructions. Cell lysates were transferred to black 96-well plates and luminescence was measured using a Veritas Microplate Luminometer (Thermo Fisher Scientific).

Cell cycle analysis

Cells were treated for 48 hours with 125 μM DFO and harvested using Trypsin (0.25%, Corning). Harvested cells were washed and fixed in 2 mL 70% ethanol (VWR, Radnor, PA) for 1 hour at 4°C. Fixed cells were washed in 2 mL FACS buffer (PBS, 5% FBS, and 0.01% sodium azide) and stained in 500 μL propidium iodide solution [0.05 mg/mL (Sigma-Aldrich, St. Louis, MO), 0.1% sodium citrate (Alfa Aesar, Heysham, England), 0.02 mg/mL RNAse (Thermo Fisher Scientific), 0.2% NP40 (Sigma-Aldrich), 1N HCl, DI water] for 1 hour at 4°C. Sample acquisition was performed using the LSR Fortessa B (BD Biosciences) with at least 10,000 events recorded per sample using the Diva software. Cell cycle analysis was performed using the ModFit LT 4.0 software (Verity Software House, Topsham, ME) in which cell counts in G1, S and G2 phases were measured.

Western blot

Cell protein was harvested using RIPA buffer (G Biosciences, St.Louis, MO) supplemented with Halt protease inhibitor (Thermo Fisher Scientific). Protein concentration was measured using the DC protein assay (Bio-rad). Electrophoretic separation of protein (12 μg/well) was performed using 4–15% gradient polyacrylamide gels (Bio-rad). Separated protein was transferred onto PVDF membranes (Bio-rad), which were then blocked for one hour at room temperature in Tris-buffered saline containing 0.1% tween (TBS-T) with 5% fat-free milk, followed by overnight incubation at 4°C with mouse anti-human HIF1-α antibody (Cell Signaling Technologies #14179S, Danvers, MA) (1:1000 dilution), goat anti-human HIF2-α antibody (1:1000 dilution) (R&D Systems #AF2997, Minneapolis, MN) or mouse anti-human β-actin antibody (1:10,000 dilution) (Cell Signaling Technology #3700S) in 5% fat-free milk with TBS-T. Membranes were washed in TBS-T and incubated for 20 minutes at room temperature with a 1:2000 dilution of horseradish peroxidase-conjugated rabbit anti-mouse antibody (Cell Signaling Technology #7076S), goat anti-rabbit antibody (Promega Life sciences #W401B), or donkey anti-goat antibody (R&D Systems #HAF109) in 5% milk with TBS-T. Protein signals were developed using the Western Sure ECL substrate (Li-cor, Lincoln, NE) or the SuperSignal West Femto Maximum Sensitive Substrate (Thermo Fisher Scientific) and measured using a C-Digit scanner (Li-cor)

RNA isolation and qPCR

Total RNA was isolated from cells treated with and without DFO for 48 hours using QIAshredders (Qiagen, Germantown, MD) and the RNEasy Mini Kit (Qiagen). Genomic DNA was digested using DNase I (Qiagen) as described in the on-column DNase digestion protocol from Qiagen. RNA concentration was determined using a Nanodrop 2000c (Thermo Fisher Scientific). One microgram of RNA was used for reverse transcription using iScript cDNA synthesis kit (Bio-Rad) according to the manufacturer's instructions. Quantitative real-time PCR was performed using iTaq Universal SYBR Green Supermix as recommended by the manufacturer (Bio-Rad). Samples were analyzed on a CFX Connect Real-Time PCR Detection system (Bio-Rad) with the following parameters: 10 min at 95°C, 40 cycles at 95°C for 15 sec and 60°C for 1 min. Melting curves were obtained by increasing temperature from 55°C to 95°C by 0.5°C increments. Data were analyzed by the $2^{\Delta\Delta CT}$ method. Primers were purchased from Integrated

DNA Technologies (IDT, Coralville, IA). Primer sequences included *B2M* forward: GGCATTCC TGAAGCTGACAG; *B2M* reverse: TGGATGACGTG AGTAAACCTG; *DIMT1* forward: TGATGTAGTGC TGGAAGTTGG, *DIMT1* reverse: GTGCCCTGAACT CTTTTGTG; *HIF-1α* (*HIF1A*) forward: AAGAACTTTTAGGCCGCTCA, *HIF-1a* reverse: CAACCCAGACATATCCACCTC; *HIF-2α* (*EPAS1*) forward: CCCATGTCTCCACCTTCAAG, *HIF-2α* reverse: GGCTTGCTCTTCATACTCCAG; *OCT4* (*POU5F1*) forward: AGAACATGTGTAAGCTGCGG, *OCT4* reverse: GTTGCCTCTCACTCGGTTC; *CA9* forward: TTTGCCAGAGTTGACGAGG, *CA9* reverse: AGCCTTCCTCAGGCATTTC; and *PDGFβ* (*PDGFB*) forward: ATGATCTCCAACGCCTGC, *PDGFβ* reverse: TCAGCAATGGTCAGGGAAC.

Statistics

Data were summarized using the mean ± standard error (SE), with comparisons between two groups made using Student's two-tailed or one-sample t-tests and comparisons made between more than two groups were done using one-way ANOVA with Tukey's post-test. Analysis was done using the GraphPad Prism software package v.6.07 (Graphpad Software Inc., San Diego, CA, USA). All statistical analyses were conducted at a significance level of 0.05.

RESULTS

Free iron levels in ccRCC and benign renal cells lines

Intracellular free iron levels were measured using the fluorescent iron chelator, Phen Green, in a panel of 4 ccRCC cell lines (786–0, A704, 769-P, RCC4) and 2 benign renal cell lines (RPTEC, HRCEp) (Figure 1). Phen Green fluorescence is quenched upon binding to iron, and its levels correlate inversely with free iron levels. Significantly lower Phen Green fluorescence was detected in all ccRCC cell lines compared to either benign renal cell line, consistent with higher free iron levels in ccRCC cells (Figure 1A, B). Because Phen Green can also bind to other divalent metals that may be present at trace levels in cells, we sought to confirm that iron was responsible for the observed differences in Phen Green fluorescence between ccRCC and benign renal cell lines. Phen Green staining was therefore re-assessed after 5-day depletion of extracellular free iron using the iron chelator, DFO. 5-day extracellular iron depletion significantly increased Phen Green fluorescence in ccRCC cell lines but not in the RPTEC and HRCEp benign renal cell lines (Figure 1C, D). Furthermore, the magnitude of dequenched fluorescence was significantly higher in each ccRCC cell line compared to RPTEC and/or HRCEp (Figure 1E). These findings support higher baseline free iron levels in ccRCC cells compared to benign renal epithelial cells.

Effects of iron deprivation on ccRCC and benign renal cell line growth

We next investigated the effect of iron deprivation on ccRCC and benign renal cell lines in MTS growth assays using two iron chelator drugs that act either extracellularly (DFO) or extracellularly and intracellularly (DFX). Treatment with either drug for 72 hours suppressed the growth of all ccRCC and benign renal cell lines at concentrations as low as <1 μM (Figure 2). Higher concentrations of DFO (>10 μM) suppressed growth in three ccRCC cell lines (786–0, 769-P, RCC4) to a much greater degree than benign renal cell

lines or the A704 ccRCC cell line (Figure 2A, B). The growth IC_{80} for DFO was reached at 11–15 μM in 786–0, 769-P and RCC4 cells (IC_{90} approached or reached at 30–60 μM), but was not reached in benign renal cell lines or A704 cells at even 10-fold higher concentrations (Figure 2A). Similar results were observed after 72-hour treatment with DFX, with the exception that A704 cells showed greater growth suppression than benign renal cell lines (Figure 2C, D). Hence, all four ccRCC cell lines were suppressed to a greater degree than the benign renal cell lines using DFX. Collectively, these data show that ccRCC cells are more sensitive than benign renal epithelial cells to growth suppression with 72-hour iron chelation; but that the A704 ccRCC cell line has much greater sensitivity to DFX than DFO. One possible explanation for the latter observation is that the speed of intracellular iron deprivation in A704 may be inadequate with extracellular-only chelation to reduce iron levels adequately within 72 hours for significant growth suppression . In this case, DFO treatment periods beyond 72 hours might be needed to reach a threshold level of A704 iron depletion that is sufficient for growth suppression relative to benign renal cell lines. To test this hypothesis, we compared growth of A704 and benign renal cells in response to a longer (120-hour) DFO treatment period. As predicted, A704 showed greater dose-dependent growth suppression relative to benign renal cell lines after 120-hour DFO treatment (Figure 2E). We also compared the speed of A704 iron depletion with DFO versus DFX at different time points over a 5-day treatment period to confirm that the latter drug is faster acting. Longer treatment with either chelator achieved greater intracellular iron deprivation; and as predicted, DFX dequenched Phen Green fluorescence significantly faster than DFO over the first 3 days, with the drugs being similarly effective by 5 days (Figure 3). These results confirm faster intracellular iron depletion with combined intracellular/extracellular iron chelation (DFX) compared to extracellular-only chelation (DFO), which may account for the difference in A704 growth sensitivity to the two drugs.

Effects of iron deprivation on apoptosis induction in ccRCC and benign renal cell lines

We next investigated whether apoptosis induction mediates growth suppression differences between ccRCC cells and benign renal cell lines in response to iron deprivation. This hypothesis was tested by measuring apoptosis levels based on Annexin V staining in a ccRCC cell line with high growth sensitivity to DFO (786–0), a ccRCC cell line with low growth sensitivity to DFO (A704), and both benign renal cell lines (RPTEC, HRCEp) (Figure 4). Apoptosis levels increased significantly in 786–0 cells but not A704 cells or benign renal cells after 48-hour DFO treatment (Figure 4A, B), consistent with cell line growth responses in the 72-hour MTS assays using DFO. Although apoptosis was not induced in A704 cells after only 48-hour DFO treatment, significant induction of A704 apoptosis was observed in association with more extensive iron deprivation using either longer extracellular chelation (120-hour DFO) (Figure 4C) or combined-extracellular/intracellular iron chelation (48-hour DFX) (Figure 4D). In contrast, both benign renal cell lines remained resistant to apoptosis induction after combined extracellular/intracellular chelation or an extended duration of extracellular chelation (Figure 4C, D). These results mirror the outcomes of our MTS assays with DFX or extended DFO treatment, and suggest that differential growth suppression of ccRCC cells relative to benign renal cell lines is due, at least in part,to apoptosis induction in ccRCC cells but not benign renal cells.

Comparison of iron deprivation effects on cell cycle phases in ccRCC and benign renal cell lines

We next tested whether cell cycle arrest contributes to ccRCC growth suppression in response to iron deprivation (Figure 5). In response to 48-hour extracellular iron chelation with DFO, the proportion of ccRCC cells in G1 phase increased significantly and the proportion in S and G2 phases decreased significantly (Figure 5), including in the A704 cell line. In contrast, benign renal cell lines showed no changes in G1, S or G2 phase distributions in response to iron chelation (Figure 5). These results indicate that ccRCC but not benign renal cell lines undergo G1 arrest as a result of iron deprivation. In contrast to the later onset of apoptosis induction, the timing of cell cycle arrest in A704 within 48 hours of DFO treatment does not correlate with the later timing of differential growth suppression in MTS assays relative to benign renal cell lines. These results suggest cell cycle arrest may contribute less than apoptosis to the differential growth suppression observed between ccRCC and benign renal cells.

Effects of iron deprivation on HIF-α expression and transcriptional activity

We next compared how HIF-1α and HIF-2α expression and transcriptional activity is altered by iron deprivation in ccRCC cell lines and benign renal cell lines. HIF-1α protein, which is absent in 786–0 and 769-P but present in A704 and RCC4 cell lines, decreased in both A704 and RCC4 in response to 48-hour extracellular chelation with DFO, in contrast to HIF-1α protein increases in benign renal cell lines (Figure 6A; supplementary Figure 1). 48-hour DFO treatment similarly led to reductions in HIF-2α protein in all ccRCC cell lines, in contrast to HIF-2α protein increases in the benign renal cell lines (Figure 6A; supplementary Figure 1). Decreased HIF-1α and HIF-2α protein levels in ccRCC cells were accompanied by HIF-1α and HIF-2α transcript upregulation, consistent with a post-transcriptional regulatory effect of iron deprivation (Figure 6B). Similarly for the benign cell lines, increases in HIF-α protein levels were for the most part accompanied by significant reduction in transcript levels, consistent with post-translational regulation (Figure 6B).

Interestingly, baseline HIF-2α (but not HIF-1α) protein levels were noted to be much higher than in A704 cells compared to other ccRCC cell lines; and even after >50% reduction with 48-hour DFO treatment, A704 HIF-2α levels remained as high as, or higher than, baseline HIF-2α levels of the other three ccRCC cell lines (Figure 6A; supplementary Figure 1). Thus, there was a correlation between HIF-2α (but not HIF-1α) protein level after 48-hour DFO treatment and ccRCC cell line resistance to DFO-induced apoptosis at 48 hours or growth suppression at 72 hours. This observation suggested the possibility that A704 apoptosis/differential growth suppression might require greater HIF-2α suppression than achieved with only 48 hours of DFO treatment. We therefore investigated whether A704 HIF-2α protein levels are further reduced under conditions sufficient for A704 apoptosis and differential growth suppression, namely either 48-hour DFX treatment or 120-hour DFO treatment. As predicted, A704 cells showed greater HIF-2α protein suppression after 120-hour DFO treatment or 48-hour DFX treatment relative to 48-hour DFO treatment (Figure 6C); and similar to suppressed HIF-2α levels achieved in other ccRCC cell lines after DFO treatment for only 48 hours (supplementary Figure 1).

To assess iron deprivation effects on HIF-α transcriptional activity, mRNA levels of HIF-α transcriptional gene targets were measured after 48-hour DFO treatment, including the HIF-2α specific target, *OCT4*, the HIF-1α specific target, *CAIX*, and the HIF-1α/HIF-2α target *PDGFβ*(Figure 6D). Iron deprivation in benign cell lines upregulated all three HIF-α target genes (Figure 6D), consistent with increases in HIF-α protein levels (Figure 6A). In contrast, iron deprivation in ccRCC cells downregulated HIF-α target genes (Figure 6D), consistent with decreases in HIF-α protein levels (Figure 6A). In the HIF-1α(−)/HIF-2α(+) 786–0 cell line, iron deprivation caused significant downregulation of the HIF-2α targets, *OCT4* and *PDGFβ*, without any effect on the HIF-1α specific target, *CA9* (Figure 6D). In the HIF-1α(+)/HIF-2α(+) A704 ccRCC cell line, iron deprivation caused significant downregulation of all HIF-α transcriptional targets; however, A704 downregulation of the HIF-2α specific target, *OCT4*, (but not HIF-1α targets) required an extended duration (120 hours) of DFO treatment (Figure 6D, E), consistent with the duration of DFO treatment required for induction of apoptosis (Figure 4C) and differential growth suppression relative to benign renal cell lines (Figure 2). These data indicate that HIF-2α protein level in A704 cells was suppressed low enough after 120-hour DFO treatment, but not 48-hour DFO treatment, for inhibition of its transcriptional activity. Collectively, these data indicate that iron deprivation suppresses HIF-α protein levels and transcriptional activity in ccRCC cells, but not in benign renal cell lines. Furthermore, the level and timing of reductions in HIF-2α but not HIF-1α protein level and transcriptional activity correlate with the level and timing of apoptosis induction and differential growth suppression, which suggests HIF-2α suppression may be important in triggering these events.

VHL loss contributes to the inhibitory effects of iron deprivation in ccRCC cells

The correlation between HIF-2α suppression and ccRCC growth suppression/apoptosis in response to iron chelation raises the possibility that ccRCC dependency on iron is mediated by HIF-2α overexpression resulting from VHL loss. To test the hypothesis that VHL loss is necessary for ccRCC dependency on iron, we performed iron chelation assays in VHL-mutant ccRCC cells stably transfected with a wild-type VHL expression vector or an empty vector control (Figure 7). Restored VHL function was confirmed by suppressed HIF-α protein levels (Figure 7A) and transcription activity (Figure 7B). Iron chelation using DFO in VHL-restored ccRCC cells increased HIF-α protein levels and transcriptional activity, in contrast to the opposite effects in VHL-inactivated ccRCC cells (Figure 7A, B). Restoration of wild-type VHL function also caused slight but significant increases in ccRCC free iron levels based on Phen Green fluorescence before and after DFO chelation (Figure 7C). Intriguingly, VHL restoration blocked induction of ccRCC apoptosis in response to iron chelation with DFO, as indicated by a significant reduction in Annexin V staining positivity (Figure 7D). To confirm this result, we also assessed apoptosis based on caspase 3 activity, which also showed a significant reduction in DFO-induced apoptosis in VHL-restored ccRCC cells relative to VHL-inactivated ccRCC cells. In contrast, VHL restoration had no effect on ccRCC caspase 3 activity in response to an alternative apoptosis-inducing drug, staurosporine (STS) (Figure 7E). These results indicate that iron deprivation-induced apoptosis in ccRCC cells is caused, at least in part, by VHL loss. Similar experiments were performed to determine whether VHL loss is also necessary for iron deprivation-induced increases in G1 cell cycle arrest. Restoration of wild-type VHL function in iron-deprived

ccRCC cells prevented the significant G1 phase increase and significant S and G2 phase decreases observed in VHL-inactivated ccRCC cells (Figure 7F). These results indicate that G1 arrest in iron-deprived ccRCC cells is, like apoptosis, dependent at least in part on VHL inactivation.

DISCUSSION

Iron has long been implicated in cancer development and progression due to its central role in oxidative stress, DNA replication and cellular proliferation in addition to several other cell processes implicated in carcinogenesis (1, 10–26). A growing body of epidemiologic and animal modeling data implicate iron accumulation in tumorigenesis of the kidney, particularly the ccRCC subtype (11, 28–33, 38, 49–51, 54, 56, 57, 59–61). Yet despite these observations, the role of iron in human ccRCC including the effects of iron deprivation on ccRCC growth and survival has remained unclear. Similarly, there has been scarce investigation into the relation between iron metabolism and VHL inactivation, which uniquely defines ccRCC (73).

The current study explored the hypothesis that ccRCC cellular iron accumulation results from an increased dependency on iron for growth and survival that is due, at least in part, to VHL/HIF-α dysregulation. Our findings confirm that ccRCC cells have higher free iron levels and increased growth susceptibility to iron deprivation compared to benign renal epithelial cells. Growth suppression in response to iron chelation was associated with apoptosis induction, G1 cell cycle arrest and reductions in HIF-1α and HIF-2α protein and transcriptional activity in ccRCC cells but not benign renal cells. Intriguingly, we also uncovered a novel interplay between ccRCC iron dependency and VHL inactivation, as restored wild-type VHL expression in VHL-mutant ccRCC cell lines was sufficient to prevent iron chelation-induced apoptosis and cell cycle arrest. These data support a novel model of ccRCC tumorigenesis in which VHL inactivation introduces iron dependency to ccRCC cells, which potentially drives their higher free iron levels.

The ability of iron chelators including DFO and DFX to suppress proliferation is described for many human cancer cell types (24, 74–86), but the current study is the first to our knowledge to do so in ccRCC. DFX depleted intracellular free iron more rapidly than DFO, consistent with its ability to act intracellularly, and caused more dramatic growth suppression in ccRCC cell lines (>90% suppression at ~30–150 μM) compared to benign renal cell lines (~10–50% suppression at up to 250 μM). Similar growth suppression was achieved using DFO, but with the notable exception that A704 sensitivity was no different than that of benign renal cell lines after short-term treatment, likely due to inadequate intracellular iron deprivation with extracellular-only chelation. Consistent with this explanation, further reductions of intracellular iron with longer durations of extracellular-only chelation differentially suppressed A704 growth relative to benign renal cells. We speculate that the lower susceptibility of the A704 cell line to extracellular iron chelation compared to other ccRCC cell lines may be due to its slower metabolism/growth rate and/or higher levels of HIF-2α protein, which required a longer duration of extracellular chelation for transcriptional activity suppression.

These findings suggest ccRCC may be uniquely susceptible to iron deprivation. DFO and DFX IC_{50} values for ccRCC cell lines other than A704 were low relative to the range of IC_{50} values reported for these drugs in other cancer cell lines (75, 82, 84–86). Whitnall et al tested DFO efficacy in a panel including 25 cell lines of 11 different cancer types, and the growth IC_{50} was above 14 μM in most cases, with only 4 (16%) cancer cell lines having an IC_{50} below 8 μM (84). Brard et al also characterized DFO responsiveness in a variety of human cancer cell lines, and each had a growth IC_{50} of at least 50 μM (82). In contrast, three of four ccRCC cell lines in our study had a growth IC_{50} of 2–4 μM DFO, which is lower than all but 2 of the >30 human cancer cell lines collectively studied by Whitnall et al and Brard et al. Similarly for DFX, IC_{50} values previously reported in 72-hour growth assays for 10 lymphoma, gastric and pancreatic cancer cell lines were higher in all cases than IC_{50} values observed in the current study for ccRCC cell lines other than A704 (75, 85, 86). We observed IC_{80} and IC_{90} values to correlate better than IC50 values with ccRCC cytotoxicity and differential growth suppression relative to benign renal cell lines. In this regard, 90% growth suppression with iron chelators is rare in prior reports, but was common in ccRCC cell lines of the current study. However, caution must be exercised in comparing cell line growth responses between different studies due to differences in experimental conditions and cell line growth rates.

Induction of ccRCC apoptosis and cell cycle arrest in response to iron chelation is consistent with previous reports in other cancer cell types. The apoptotic program induced by iron chelators has been characterized as Fas ligand-independent, mitochondria-based apoptosis mediated by cytochrome c and caspase 3 (78, 82, 87–89). Cell cycle arrest in response to iron chelators classically includes blockage in G1 and/or S phases, the latter of which is due to RR enzyme/DNA synthesis inhibition (23), and the former of which is associated with cyclin-dependent kinase 2 suppression and increases in cyclin E but not cyclins A, B or D1 (14, 16, 20, 23). In the current study, elevations in caspase 3 were observed during ccRCC apoptosis, which is consistent with a mitochondrial apoptotic program. We did not detect S phase arrest, however the degree of G1 arrest in ccRCC cells may have masked S arrest by preventing G1/S transition (23). Consistent with our findings, Brodie et al observed that G1 arrest rather than S arrest was associated with greater growth susceptibility to iron chelation (90). Although the relative contribution of cell cycle arrest versus apoptosis to chelator-induced growth suppression is unclear, apoptosis has been suggested by others to be the more important mechanism in other cell types (89). Our data support a similar possibility in ccRCC, since the timing of apoptosis induction correlated better than the timing of cell cycle arrest with the onset of differential growth inhibition relative to benign renal cells.

HIF-α suppression in response to ccRCC iron chelation is novel among cancers studied to date and can be attributed to VHL inactivation that occurs uniquely in this cancer type. Under physiologic conditions, iron regulates HIF-α expression by two independent mechanisms: 1) IRE-dependent increase in translation of the HIF-2α (and possibly HIF-1α) transcript (66, 91); and 2) activation of PHD to catalyze VHL-dependent HIF-α protein degradation (38). The latter mechanism is the more potent under normal conditions, and hence iron chelation usually causes HIF-α protein accumulation despite reduced IRE-dependent translation, as occurred in benign renal cell lines in the current study. In contrast, the inactivated VHL/PHD complex in ccRCC cells prevents PHD-dependent

stabilization of HIF-α protein in response to iron chelation, and enables IRE-mediated HIF-α suppression to manifest instead (66). In the current study, reduction in HIF-1α and HIF-2α proteins occurred with ccRCC iron chelation despite HIF-α transcript upregulation, which is consistent with the IRE-dependent post-transcriptional suppression mechanism. This result was unexpected for HIF-1α because a “near consensus” IRE motif in the HIF-1α transcript has not been functionally confirmed (91), in contrast to the IRE for HIF-2α (66). Our observations provide novel support for a functionally active IRE in HIF-1α, although alternative post-transcriptional mechanisms may be responsible since iron affects so many enzymes and signaling pathways. Consistent with a functional HIF-1α IRE, Sourbier et al observed the IRP1-activating drug, Tempol, to suppress protein levels of not only HIF-2α, but also HIF-1α (92).

Given the known requirement for HIF-2α protein accumulation in ccRCC tumorigenesis, we speculate that a need for iron to optimally augment HIF-2α accumulation might be mechanistically responsible, at least in part, for the dependency of ccRCC on iron for growth and survival. Animal models and clinical studies of germline VHL-mutant ccRCC indicate that VHL mutation alone is insufficient for tumorigenesis or HIF-α accumulation to levels observed in ccRCC cells, supporting the need for other alterations, such as free iron accumulation (93–96). Consistent with a role for HIF-2α suppression in chelator-induced ccRCC growth suppression, induction of differential growth suppression and apoptosis correlated well with the level and timing of HIF-2α suppression. Furthermore, reversal of chelator-induced HIF-2α suppression with wild-type VHL restoration was associated with lost apoptotic and growth arrest susceptibility to iron chelation. Whether the suppressive effect of iron deprivation might be mediated also by HIF-1α reductions is unclear, however several observations by us and others challenge this possibility. First, all four ccRCC cell lines in this study expressed HIF-2α, whereas only two ccRCC cell lines expressed HIF-1α, consistent with reported rates of HIF-2α and HIF-1α expression in ccRCC patient tumors (43). Second, the timing and level of HIF-1α suppression in these two HIF-1α(+) ccRCC cell lines did not correlate consistently with the induction of apoptosis or differential growth suppression. Third, HIF-1α does not contribute to ccRCC cell line tumorigenic properties (44, 45) and instead appears to have ccRCC tumor suppressor function (97).

An intriguing conclusion of our experiments in ccRCC cells with and without wild-type VHL restoration is that VHL inactivation simultaneously lowers iron levels while increasing iron dependency. Therefore, high free iron levels in ccRCC cells must result from other unidentified alterations, independent of VHL inactivation. Such alterations would presumably impart a selective advantage to VHL-inactivated cells due to these cells’ tendency for lower iron levels yet higher susceptibility to iron depletion. Consistent with this idea, Alberghini et al too concluded that VHL inactivation reduces ccRCC cellular free iron (73). Interestingly, they also noted a paradoxical increase in stored (non-free) iron as a result of VHL inactivation, leading to the conclusion that VHL inactivation increases efficiency of ferritin iron storage by unknown mechanisms (73). Clearly, the interplay between iron metabolism and VHL inactivation is complex and requires further study of the dynamic interaction between free and stored iron pools. A recent study by Miess et al has shown that VHL inactivation increases ccRCC sensitivity to ferroptosis, which supports the interplay between VHL inactivation and iron metabolism in ccRCC (98).

In addition to the important role of VHL inactivation, it is likely that VHL/HIF-α independent pathways simultaneously mediate ccRCC susceptibility to iron deprivation. Several studies indicate that reversal of HIF-1α or HIF-2α accumulation is alone inadequate for *in vitro* growth suppression of ccRCC cell lines (44, 45, 99). Hence, mechanisms that are independent of (but perhaps cooperate with) HIF-α suppression may be necessary for iron-deprivation to inhibit ccRCC growth. HIF-α independent iron chelator-induced molecular events that might mediate this role include the induction of chromatin remodeling and inhibition of DNA repair (12, 22), both of which are well implicated in ccRCC tumorigenesis (37). Furthermore, ccRCC is uniquely characterized by metabolic perturbations (38), which are likely to be affected by iron deprivation since iron is a cofactor for a variety of metabolic enzyme classes, including catalases, peroxidases, cytochromes, desaturases and aconitase (19). Other HIF-α independent mechanisms triggered by iron chelation that might suppress cancer growth include: endoplasmic reticulum stress induction (15) with upregulation of stress-activated protein kinases (18, 25) and autophagy modulation (13, 17, 21); suppression of epithelial-to-mesenchymal transition (18, 100); IFN-gamma activation (101, 102); wide-spread promoter methylation (24); and modulation of pathways involving FAK/Pyk2/Src, Wnt/beta-catenin, COX2 or NDRG1 (17, 103–105). Determining which, if any, of these diverse mechanisms might cooperate with HIF-α suppression to mediate ccRCC iron dependency represents an important area for future research.

An intriguing implication of this work is the possibility of clinically exploiting ccRCC cellular iron as a novel therapeutic target. Current clinical therapeutics for advanced RCC patients that indirectly target the VHL/HIF-α axis improve patient survival only modestly (48). While initial efforts to directly target HIF-2α led to the frustrating conclusion that this protein is “undruggable” (106), more recently developed small molecule inhibitors have yielded promising early results (106–108). Intriguingly, certain drugs that lower HIF-2α levels have been suggested to work through reduction of iron levels (91). Given our findings of ccRCC dependency on iron for HIF-2α overexpression, growth and survival, iron chelators and other pharmaceutical approaches for lowering iron may have therapeutic efficacy in ccRCC patients. Both DFO and DFX are already approved for clinical use in systemic iron overload conditions and have demonstrated safety in patients, including at doses sufficient to generate steady-state serum concentrations well within the range tested here in ccRCC cell lines (67, 68). Whereas DFO clinical use has been historically limited by a need for parental intravenous dosing, the more recent advent of orally administered iron chelators, DFX and deferiprone (DFP), has made daily iron chelator administration feasible. Moreover, dual oral chelator combination therapy (DFX + DFP) has proven safe and effective for lowering iron stores in patients with suboptimal responses to monotherapy (69, 70). Encouragingly, there is reported an oncologic benefit of iron chelation as monotherapy or as a chemotherapeutic adjuvant for hepatocellular carcinoma and neuroblastoma patients, respectively (71, 72). However, investigational use of these drugs in cancer patients has been limited by low-grade toxicity (79, 109). Although iron chelation did not induce apoptosis or growth arrest of benign renal cells in this study, the *in vivo* consequences of HIF-α upregulation in benign renal epithelium as a result of iron chelator treatment require further characterization to determine potential contributions to nephrotoxicity and even malignant transformation risk. In the interim, newer generation iron chelator drugs may provide more

effective and safer iron reductions, but require further preclinical and clinical validation (88, 110–113). Finally, strategies to lower iron selectively in ccRCC tumors, including by targeting TfR1, may complement current non-specific iron chelation approaches and warrant future investigation (28).

CONCLUSIONS

Despite a growing body of research implicating iron in human carcinogenesis, the actual impact and underlying mechanisms remain unclear. We believe there is compelling preclinical and clinical data to support a uniquely important role for iron in ccRCC tumorigenesis, particularly given the interplay between iron metabolism and the VHL/HIF-α axis, whose dysregulation underlies this cancer. The current study provides novel evidence of free iron accumulation in ccRCC cells and a heightened dependency of ccRCC on iron for cell cycle progression and apoptotic escape due, at least in part, to VHL/HIF-α dysregulation. The level of growth suppression in ccRCC cells with iron chelation suggests this cancer may be particularly sensitive to iron deprivation strategies. Future studies are warranted to dissect the molecular mechanisms mediating iron deprivation effects in ccRCC, including confirmation of a central role for HIF-2α and identification of key cooperating pathways. In the interim, the most intriguing implication of this work is the possibility of clinically exploiting ccRCC iron dependency as a novel therapeutic target to suppress HIF-2α and cancer progression in ccRCC patients.

Supplementary Material

Refer to Web version on PubMed Central for supplementary material.

FUNDING/SUPPORT

This research is funded by an Intramural Research Grant from the American Cancer Society, a RPCCC Alliance Foundation grant, and generous support from the Bruce Moden family. Flow cytometry work was supported by a RPCCC Flow and Imaging Shared Resource, which is funded by the National Cancer Institute (NCI) Cancer Center Support Grant P30CA016056.

ABBREVIATIONS

ccRCC	Clear cell RCC
DFO	Deferoxamine
DFX	Deferasirox
HIF-α	Hypoxia inducible factor-α
HIF-1α	Hypoxia inducible factor 1-α
HIF-2α	Hypoxia inducible factor 2-α
IRE	Iron responsive element
IRP1/ACO1	Iron regulatory protein 1

NCI	National cancer institute
PHD	Prolyl hydroxylase
RCC	Renal cell carcinoma
ROS	Reactive oxygen species
RPCCC	Roswell Park Comprehensive Cancer Center
TfR1/TFRC	Transferrin receptor 1
VHL	von Hippel Lindau

REFERENCES

1. Galy B, Ferring-Appel D, Sauer SW, Kaden S, Lyoumi S, Puy H, et al. Iron regulatory proteins secure mitochondrial iron sufficiency and function. Cell Metab. 2010;12(2):194–201. [PubMed: 20674864]
2. Muto Y, Nishiyama M, Nita A, Moroishi T, Nakayama KI. Essential role of FBXL5-mediated cellular iron homeostasis in maintenance of hematopoietic stem cells. Nat Commun. 2017;8:16114.
3. Ohira Y, Gill SL. Effects of dietary iron deficiency on muscle fiber characteristics and whole-body distribution of hemoglobin in mice. J Nutr. 1983;113(9):1811–8. [PubMed: 6886825]
4. Netz DJ, Stith CM, Stumpfig M, Kopf G, Vogel D, Genau HM, et al. Eukaryotic DNA polymerases require an iron-sulfur cluster for the formation of active complexes. Nat Chem Biol. 2011;8(1):125–32. [PubMed: 22119860]
5. Schuth N, Mebs S, Huwald D, Wrzolek P, Schwalbe M, Hemschemeier A, et al. Effective intermediate-spin iron in O2-transporting heme proteins. Proc Natl Acad Sci U S A. 2017;114(32):8556–61. [PubMed: 28739893]
6. Kruszewski M. Labile iron pool: the main determinant of cellular response to oxidative stress. Mutat Res. 2003;531(1–2):81–92. [PubMed: 14637247]
7. Lipinski P, Drapier JC, Oliveira L, Retmanska H, Sochanowicz B, Kruszewski M. Intracellular iron status as a hallmark of mammalian cell susceptibility to oxidative stress: a study of L5178Y mouse lymphoma cell lines differentially sensitive to H(2)O(2). Blood. 2000;95(9):2960–6. [PubMed: 10779446]
8. Inoue S, Kawanishi S. Hydroxyl radical production and human DNA damage induced by ferric nitrilotriacetate and hydrogen peroxide. Cancer Res. 1987;47(24 Pt 1):6522–7. [PubMed: 2824034]
9. Dizdaroglu M, Jaruga P. Mechanisms of free radical-induced damage to DNA. Free Radic Res. 2012;46(4):382–419. [PubMed: 22276778]
10. Toyokuni S. Oxidative stress as an iceberg in carcinogenesis and cancer biology. Arch Biochem Biophys. 2016;595:46–9. [PubMed: 27095214]
11. Toyokuni S. The origin and future of oxidative stress pathology: From the recognition of carcinogenesis as an iron addiction with ferroptosis-resistance to non-thermal plasma therapy. Pathol Int. 2016;66(5):245–59. [PubMed: 26931176]
12. Benadiba J, Rosilio C, Nebout M, Heimeroth V, Neffati Z, Popa A, et al. Iron chelation: an adjuvant therapy to target metabolism, growth and survival of murine PTEN-deficient T lymphoma and human T lymphoblastic leukemia/lymphoma. Leuk Lymphoma. 2017;58(6):1433–45. [PubMed: 27736268]
13. Castino R, Fiorentino I, Cagnin M, Giovia A, Isidoro C. Chelation of lysosomal iron protects dopaminergic SH-SY5Y neuroblastoma cells from hydrogen peroxide toxicity by precluding autophagy and Akt dephosphorylation. Toxicol Sci. 2011;123(2):523–41. [PubMed: 21742779]
14. Gao J, Richardson DR. The potential of iron chelators of the pyridoxal isonicotinoyl hydrazone class as effective antiproliferative agents, IV: The mechanisms involved in inhibiting cell-cycle progression. Blood. 2001;98(3):842–50. [PubMed: 11468187]

15. Kim JL, Lee DH, Na YJ, Kim BR, Jeong YA, Lee SI, et al. Iron chelator-induced apoptosis via the ER stress pathway in gastric cancer cells. Tumour Biol. 2016;37(7):9709–19. [PubMed: 26803514]
16. Kulp KS, Green SL, Vulliet PR. Iron deprivation inhibits cyclin-dependent kinase activity and decreases cyclin D/CDK4 protein levels in asynchronous MDA-MB-453 human breast cancer cells. Exp Cell Res. 1996;229(1):60–8. [PubMed: 8940249]
17. Lane DJ, Saletta F, Suryo Rahmanto Y, Kovacevic Z, Richardson DR. N-myc downstream regulated 1 (NDRG1) is regulated by eukaryotic initiation factor 3a (eIF3a) during cellular stress caused by iron depletion. PLoS One. 2013;8(2):e57273.
18. Lee SK, Jang HJ, Lee HJ, Lee J, Jeon BH, Jun CD, et al. p38 and ERK MAP kinase mediates iron chelator-induced apoptosis and -suppressed differentiation of immortalized and malignant human oral keratinocytes. Life Sci. 2006;79(15):1419–27. [PubMed: 16697418]
19. Lieu PT, Heiskala M, Peterson PA, Yang Y. The roles of iron in health and disease. Mol Aspects Med. 2001;22(1–2):1–87. [PubMed: 11207374]
20. Liu Y, Templeton DM. Iron-loaded cardiac myocytes stimulate cardiac myofibroblast DNA synthesis. Mol Cell Biochem. 2006;281(1–2):77–85. [PubMed: 16328959]
21. Moon JH, Jeong JK, Park SY. Deferoxamine inhibits TRAIL-mediated apoptosis via regulation of autophagy in human colon cancer cells. Oncol Rep. 2015;33(3):1171–6. [PubMed: 25524470]
22. Pogribny IP, Tryndyak VP, Pogribna M, Shpyleva S, Surratt G, Gamboa da Costa G, et al. Modulation of intracellular iron metabolism by iron chelation affects chromatin remodeling proteins and corresponding epigenetic modifications in breast cancer cells and increases their sensitivity to chemotherapeutic agents. Int J Oncol. 2013;42(5):1822–32. [PubMed: 23483119]
23. Siriwardana G, Seligman PA. Two cell cycle blocks caused by iron chelation of neuroblastoma cells: separating cell cycle events associated with each block. Physiol Rep. 2013;1(7):e00176.
24. Cao LL, Liu H, Yue Z, Liu L, Pei L, Gu J, et al. Iron chelation inhibits cancer cell growth and modulates global histone methylation status in colorectal cancer. Biometals. 2018;31(5):797–805. [PubMed: 29951879]
25. Yu Y, Richardson DR. Cellular iron depletion stimulates the JNK and p38 MAPK signaling transduction pathways, dissociation of ASK1-thioredoxin, and activation of ASK1. J Biol Chem. 2011;286(17):15413–27.
26. Steegmann-Olmedillas JL. The role of iron in tumour cell proliferation. Clin Transl Oncol. 2011;13(2):71–6. [PubMed: 21324793]
27. Cloonan SM, Glass K, Laucho-Contreras ME, Bhashyam AR, Cervo M, Pabon MA, et al. Mitochondrial iron chelation ameliorates cigarette smoke-induced bronchitis and emphysema in mice. Nat Med. 2016;22(2):163–74. [PubMed: 26752519]
28. Greene CJ, Attwood K, Sharma NJ, Gross KW, Smith GJ, Xu B, et al. Transferrin receptor 1 upregulation in primary tumor and downregulation in benign kidney is associated with progression and mortality in renal cell carcinoma patients. Oncotarget. 2017;8(63):107052–75.
29. Mandel JS, McLaughlin JK, Schlehofer B, Mellemgaard A, Helmert U, Lindblad P, et al. International renal-cell cancer study. IV. Occupation. Int J Cancer. 1995;61(5):601–5. [PubMed: 7768630]
30. McCredie M, Stewart JH. Risk factors for kidney cancer in New South Wales. IV. Occupation. Br J Ind Med. 1993;50(4):349–54. [PubMed: 8494775]
31. Partanen T, Heikkila P, Hernberg S, Kauppinen T, Moneta G, Ojajarvi A. Renal cell cancer and occupational exposure to chemical agents. Scand J Work Environ Health. 1991;17(4):231–9. [PubMed: 1925434]
32. Ricchi P, Ammirabile M, Spasiano A, Costantini S, Di Matola T, Carteni G, et al. Renal cell carcinoma in adult patients with thalassaemia major: a description of three cases. Br J Haematol. 2014;165(6):887–8. [PubMed: 24571286]
33. Seminog OO, Ogunlaja OI, Yeates D, Goldacre MJ. Risk of individual malignant neoplasms in patients with sickle cell disease: English national record linkage study. J R Soc Med. 2016;109(8):303–9. [PubMed: 27325377]
34. Weinberg ED. Tobacco smoke iron: an initiator/promoter of multiple diseases. Biometals. 2009;22(2):207–10. [PubMed: 18704272]

35. Siegel RL, Miller KD, Jemal A. Cancer Statistics, 2017. CA Cancer J Clin. 2017;67(1):7–30. [PubMed: 28055103]
36. Gandaglia G, Ravi P, Abdollah F, Abd-El-Barr AE, Becker A, Popa I, et al. Contemporary incidence and mortality rates of kidney cancer in the United States. Can Urol Assoc J. 2014;8(7–8):247–52. [PubMed: 25210548]
37. Cancer Genome Atlas Research N. Comprehensive molecular characterization of clear cell renal cell carcinoma. Nature. 2013;499(7456):43–9. [PubMed: 23792563]
38. Linehan WM, Ricketts CJ. The metabolic basis of kidney cancer. Semin Cancer Biol. 2013;23(1):46–55. [PubMed: 22705279]
39. Cancer Genome Atlas Research N, Linehan WM, Spellman PT, Ricketts CJ, Creighton CJ, Fei SS, et al. Comprehensive Molecular Characterization of Papillary Renal-Cell Carcinoma. N Engl J Med. 2016;374(2):135–45. [PubMed: 26536169]
40. Davis CF, Ricketts CJ, Wang M, Yang L, Cherniack AD, Shen H, et al. The somatic genomic landscape of chromophobe renal cell carcinoma. Cancer Cell. 2014;26(3):319–30. [PubMed: 25155756]
41. Gnarra JR, Tory K, Weng Y, Schmidt L, Wei MH, Li H, et al. Mutations of the VHL tumour suppressor gene in renal carcinoma. Nature genetics. 1994;7(1):85–90. [PubMed: 7915601]
42. Moore LE, Nickerson ML, Brennan P, Toro JR, Jaeger E, Rinsky J, et al. Von Hippel-Lindau (VHL) inactivation in sporadic clear cell renal cancer: associations with germline VHL polymorphisms and etiologic risk factors. PLoS genetics. 2011;7(10):e1002312.
43. Gordan JD, Lal P, Dondeti VR, Letrero R, Parekh KN, Oquendo CE, et al. HIF-alpha effects on c-Myc distinguish two subtypes of sporadic VHL-deficient clear cell renal carcinoma. Cancer Cell. 2008;14(6):435–46. [PubMed: 19061835]
44. Kondo K, Klco J, Nakamura E, Lechpammer M, Kaelin WG, Jr. Inhibition of HIF is necessary for tumor suppression by the von Hippel-Lindau protein. Cancer Cell. 2002;1(3):237–46. [PubMed: 12086860]
45. Maranchie JK, Vasselli JR, Riss J, Bonifacino JS, Linehan WM, Klausner RD. The contribution of VHL substrate binding and HIF1-alpha to the phenotype of VHL loss in renal cell carcinoma. Cancer Cell. 2002;1(3):247–55. [PubMed: 12086861]
46. Singer EA, Gupta GN, Srinivasan R. Targeted therapeutic strategies for the management of renal cell carcinoma. Current opinion in oncology. 2012;24(3):284–90. [PubMed: 22343386]
47. Choueiri TK, Motzer RJ. Systemic Therapy for Metastatic Renal-Cell Carcinoma. The New England journal of medicine. 2017;376(4):354–66. [PubMed: 28121507]
48. Molina AM, Motzer RJ. Clinical practice guidelines for the treatment of metastatic renal cell carcinoma: today and tomorrow. The oncologist. 2011;16 Suppl 2:45–50. [PubMed: 21346039]
49. Ekblom P, Thesleff I, Saxen L, Miettinen A, Timpl R. Transferrin as a fetal growth factor: acquisition of responsiveness related to embryonic induction. Proc Natl Acad Sci U S A. 1983;80(9):2651–5. [PubMed: 6405384]
50. Fujishiro H, Yano Y, Takada Y, Tanihara M, Himeno S. Roles of ZIP8, ZIP14, and DMT1 in transport of cadmium and manganese in mouse kidney proximal tubule cells. Metallomics. 2012;4(7):700–8. [PubMed: 22534978]
51. Meyron-Holtz EG, Ghosh MC, Iwai K, LaVaute T, Brazzolotto X, Berger UV, et al. Genetic ablations of iron regulatory proteins 1 and 2 reveal why iron regulatory protein 2 dominates iron homeostasis. EMBO J. 2004;23(2):386–95. [PubMed: 14726953]
52. May ME, Parmley RT, Spicer SS, Ravenel DP, May EE, Buse MG. Iron nitrilotriacetate--induced experimental diabetes in rats. J Lab Clin Med. 1980;95(4):525–35. [PubMed: 6987319]
53. Queiroz-Andrade M, Blasbalg R, Ortega CD, Rodstein MA, Baroni RH, Rocha MS, et al. MR imaging findings of iron overload. Radiographics. 2009;29(6):1575–89. [PubMed: 19959509]
54. Wei H, Ke HL, Lin J, Shete S, Wood CG, Hildebrandt MA. MicroRNA target site polymorphisms in the VHL-HIF1alpha pathway predict renal cell carcinoma risk. Mol Carcinog. 2014;53(1):1–7. [PubMed: 22517515]
55. Tajima S, Ikeda Y, Enomoto H, Imao M, Horinouchi Y, Izawa-Ishizawa Y, et al. Angiotensin II alters the expression of duodenal iron transporters, hepatic hepcidin, and body iron distribution in mice. Eur J Nutr. 2015;54(5):709–19. [PubMed: 25096756]

56. Li JL, Okada S, Hamazaki S, Ebina Y, Midorikawa O. Subacute nephrotoxicity and induction of renal cell carcinoma in mice treated with ferric nitrilotriacetate. Cancer research. 1987;47(7):1867–9. [PubMed: 3815378]
57. Vargas-Olvera CY, Sanchez-Gonzalez DJ, Solano JD, Aguilar-Alonso FA, Montalvo-Munoz F, Martinez-Martinez CM, et al. Characterization of N-diethylnitrosamine-initiated and ferric nitrilotriacetate-promoted renal cell carcinoma experimental model and effect of a tamarind seed extract against acute nephrotoxicity and carcinogenesis. Molecular and cellular biochemistry. 2012;369(1–2):105–17. [PubMed: 22761015]
58. Ebina Y, Okada S, Hamazaki S, Ogino F, Li JL, Midorikawa O. Nephrotoxicity and renal cell carcinoma after use of iron- and aluminum-nitrilotriacetate complexes in rats. Journal of the National Cancer Institute. 1986;76(1):107–13. [PubMed: 3455733]
59. Iqbal M, Okazaki Y, Okada S. Curcumin attenuates oxidative damage in animals treated with a renal carcinogen, ferric nitrilotriacetate (Fe-NTA): implications for cancer prevention. Molecular and cellular biochemistry. 2009;324(1–2):157–64. [PubMed: 19165575]
60. Li GH, Akatsuka S, Chew SH, Jiang L, Nishiyama T, Sakamoto A, et al. Fenton reaction-induced renal carcinogenesis in Mutyh-deficient mice exhibits less chromosomal aberrations than the rat model. Pathol Int. 2017;67(11):564–74. [PubMed: 29027306]
61. Mukaide T, Hattori Y, Misawa N, Funahashi S, Jiang L, Hirayama T, et al. Histological detection of catalytic ferrous iron with the selective turn-on fluorescent probe RhoNox-1 in a Fenton reaction-based rat renal carcinogenesis model. Free Radic Res. 2014;48(9):990–5. [PubMed: 24580501]
62. Akatsuka S, Yamashita Y, Ohara H, Liu YT, Izumiya M, Abe K, et al. Fenton reaction induced cancer in wild type rats recapitulates genomic alterations observed in human cancer. PLoS One. 2012;7(8):e43403.
63. Mastrogiannaki M, Matak P, Keith B, Simon MC, Vaulont S, Peyssonnaux C. HIF-2alpha, but not HIF-1alpha, promotes iron absorption in mice. J Clin Invest. 2009;119(5):1159–66. [PubMed: 19352007]
64. Yang L, Wang D, Wang XT, Lu YP, Zhu L. The roles of hypoxia-inducible Factor-1 and iron regulatory protein 1 in iron uptake induced by acute hypoxia. Biochem Biophys Res Commun. 2018;507(1–4):128–35. [PubMed: 30415773]
65. Abboud S, Haile DJ. A novel mammalian iron-regulated protein involved in intracellular iron metabolism. J Biol Chem. 2000;275(26):19906–12.
66. Sanchez M, Galy B, Muckenthaler MU, Hentze MW. Iron-regulatory proteins limit hypoxia-inducible factor-2alpha expression in iron deficiency. Nat Struct Mol Biol. 2007;14(5):420–6. [PubMed: 17417656]
67. Saliba AN, El Rassi F, Taher AT. Clinical monitoring and management of complications related to chelation therapy in patients with beta-thalassemia. Expert Rev Hematol. 2016;9(2):151–68. [PubMed: 26613264]
68. Sridharan K, Sivaramakrishnan G. Efficacy and safety of iron chelators in thalassemia and sickle cell disease: a multiple treatment comparison network meta-analysis and trial sequential analysis. Expert Rev Clin Pharmacol. 2018;11(6):641–50. [PubMed: 29727586]
69. Totadri S, Bansal D, Bhatia P, Attri SV, Trehan A, Marwaha RK. The deferiprone and deferasirox combination is efficacious in iron overloaded patients with beta-thalassemia major: A prospective, single center, open-label study. Pediatr Blood Cancer. 2015;62(9):1592–6. [PubMed: 25820920]
70. El-Beshlawy A, Manz C, Naja M, Eltagui M, Tarabishi C, Youssry I, et al. Iron chelation in thalassemia: combined or monotherapy? The Egyptian experience. Ann Hematol. 2008;87(7):545–50. [PubMed: 18351337]
71. Yamasaki T, Terai S, Sakaida I. Deferoxamine for advanced hepatocellular carcinoma. The New England journal of medicine. 2011;365(6):576–8. [PubMed: 21830988]
72. Donfrancesco A, Deb G, Dominici C, De Sio L, Inserra A, Boglino C, et al. D-CECaT as preoperative chemotherapy for unresectable neuroblastoma in children over one year of age. Anticancer Res. 1995;15(5B):2347–50. [PubMed: 8572650]
73. Alberghini A, Recalcati S, Tacchini L, Santambrogio P, Campanella A, Cairo G. Loss of the von Hippel Lindau tumor suppressor disrupts iron homeostasis in renal carcinoma cells. J Biol Chem. 2005;280(34):30120–8.

74. Shinoda S, Kaino S, Amano S, Harima H, Matsumoto T, Fujisawa K, et al. Deferasirox, an oral iron chelator, with gemcitabine synergistically inhibits pancreatic cancer cell growth in vitro and in vivo. Oncotarget. 2018;9(47):28434–44.
75. Harima H, Kaino S, Takami T, Shinoda S, Matsumoto T, Fujisawa K, et al. Deferasirox, a novel oral iron chelator, shows antiproliferative activity against pancreatic cancer in vitro and in vivo. BMC Cancer. 2016;16:702. [PubMed: 27582255]
76. Tury S, Assayag F, Bonin F, Chateau-Joubert S, Servely JL, Vacher S, et al. The iron chelator deferasirox synergises with chemotherapy to treat triple-negative breast cancers. J Pathol. 2018.
77. Yang DC, Jiang XP, Elliott RL, Head JF. Inhibition of growth of human breast carcinoma cells by an antisense oligonucleotide targeted to the transferrin receptor gene. Anticancer Res. 2001;21(3B):1777–87. [PubMed: 11497259]
78. Lee DH, Jang PS, Chung NG, Cho B, Jeong DC, Kim HK. Deferasirox shows in vitro and in vivo antileukemic effects on murine leukemic cell lines regardless of iron status. Exp Hematol. 2013;41(6):539–46. [PubMed: 23415674]
79. Saeki I, Yamamoto N, Yamasaki T, Takami T, Maeda M, Fujisawa K, et al. Effects of an oral iron chelator, deferasirox, on advanced hepatocellular carcinoma. World J Gastroenterol. 2016;22(40):8967–77. [PubMed: 27833388]
80. Ford SJ, Obeidy P, Lovejoy DB, Bedford M, Nichols L, Chadwick C, et al. Deferasirox (ICL670A) effectively inhibits oesophageal cancer growth in vitro and in vivo. Br J Pharmacol. 2013;168(6):1316–28. [PubMed: 23126308]
81. Lee JC, Chiang KC, Feng TH, Chen YJ, Chuang ST, Tsui KH, et al. The Iron Chelator, Dp44mT, Effectively Inhibits Human Oral Squamous Cell Carcinoma Cell Growth in Vitro and in Vivo. Int J Mol Sci. 2016;17(9).
82. Brard L, Granai CO, Swamy N. Iron chelators deferoxamine and diethylenetriamine pentaacetic acid induce apoptosis in ovarian carcinoma. Gynecol Oncol. 2006;100(1):116–27. [PubMed: 16203029]
83. Shen L, Zhao HY, Du J, Wang F. Anti-tumor activities of four chelating agents against human neuroblastoma cells. In Vivo. 2005;19(1):233–6. [PubMed: 15796180]
84. Whitnall M, Howard J, Ponka P, Richardson DR. A class of iron chelators with a wide spectrum of potent antitumor activity that overcomes resistance to chemotherapeutics. Proc Natl Acad Sci U S A. 2006;103(40):14901–6. [PubMed: 17003122]
85. Tabor E, Kim CM. Inhibition of human hepatocellular carcinoma and hepatoblastoma cell lines by deferoxamine. J Med Virol. 1991;34(1):45–50. [PubMed: 1715897]
86. Chang YC, Lo WJ, Huang YT, Lin CL, Feng CC, Lin HT, et al. Deferasirox has strong anti-leukemia activity but may antagonize theanti-leukemia effect of doxorubicin. Leuk Lymphoma. 2017;58(9):1–12.
87. Greene BT, Thorburn J, Willingham MC, Thorburn A, Planalp RP, Brechbiel MW, et al. Activation of caspase pathways during iron chelator-mediated apoptosis. J Biol Chem. 2002;277(28):25568–75.
88. Noulsri E, Richardson DR, Lerdwana S, Fucharoen S, Yamagishi T, Kalinowski DS, et al. Antitumor activity and mechanism of action of the iron chelator, Dp44mT, against leukemic cells. Am J Hematol. 2009;84(3):170–6. [PubMed: 19140186]
89. Lee SK, Lee JJ, Lee HJ, Lee J, Jeon BH, Jun CD, et al. Iron chelator-induced growth arrest and cytochrome c-dependent apoptosis in immortalized and malignant oral keratinocytes. J Oral Pathol Med. 2006;35(4):218–26. [PubMed: 16519769]
90. Brodie C, Siriwardana G, Lucas J, Schleicher R, Terada N, Szepesi A, et al. Neuroblastoma sensitivity to growth inhibition by deferrioxamine: evidence for a block in G1 phase of the cell cycle. Cancer Res. 1993;53(17):3968–75. [PubMed: 8358725]
91. Zimmer M, Ebert BL, Neil C, Brenner K, Papaioannou I, Melas A, et al. Small-molecule inhibitors of HIF-2a translation link its 5'UTR iron-responsive element to oxygen sensing. Mol Cell. 2008;32(6):838–48. [PubMed: 19111663]
92. Sourbier C, Srivastava G, Ghosh MC, Ghosh S, Yang Y, Gupta G, et al. Targeting HIF2alpha translation with Tempol in VHL-deficient clear cell renal cell carcinoma. Oncotarget. 2012;3(11):1472–82. [PubMed: 23178531]

93. Haase VH, Glickman JN, Socolovsky M, Jaenisch R. Vascular tumors in livers with targeted inactivation of the von Hippel-Lindau tumor suppressor. Proc Natl Acad Sci U S A. 2001;98(4):1583–8. [PubMed: 11171994]
94. Kleymenova E, Everitt JI, Pluta L, Portis M, Gnarra JR, Walker CL. Susceptibility to vascular neoplasms but no increased susceptibility to renal carcinogenesis in Vhl knockout mice. Carcinogenesis. 2004;25(3):309–15. [PubMed: 14604887]
95. Rankin EB, Tomaszewski JE, Haase VH. Renal cyst development in mice with conditional inactivation of the von Hippel-Lindau tumor suppressor. Cancer Res. 2006;66(5):2576–83. [PubMed: 16510575]
96. Mandriota SJ, Turner KJ, Davies DR, Murray PG, Morgan NV, Sowter HM, et al. HIF activation identifies early lesions in VHL kidneys: evidence for site-specific tumor suppressor function in the nephron. Cancer Cell. 2002;1(5):459–68. [PubMed: 12124175]
97. Shen C, Beroukhim R, Schumacher SE, Zhou J, Chang M, Signoretti S, et al. Genetic and functional studies implicate HIF1alpha as a 14q kidney cancer suppressor gene. Cancer Discov. 2011;1(3):222–35. [PubMed: 22037472]
98. Miess H, Dankworth B, Gouw AM, Rosenfeldt M, Schmitz W, Jiang M, et al. The glutathione redox system is essential to prevent ferroptosis caused by impaired lipid metabolism in clear cell renal cell carcinoma. Oncogene. 2018;37(40):5435–50. [PubMed: 29872221]
99. Shinojima T, Oya M, Takayanagi A, Mizuno R, Shimizu N, Murai M. Renal cancer cells lacking hypoxia inducible factor (HIF)-1alpha expression maintain vascular endothelial growth factor expression through HIF-2alpha. Carcinogenesis. 2007;28(3):529–36. [PubMed: 16920734]
100. Chen Z, Zhang D, Yue F, Zheng M, Kovacevic Z, Richardson DR. The iron chelators Dp44mT and DFO inhibit TGF-beta-induced epithelial-mesenchymal transition via up-regulation of N-Myc downstream-regulated gene 1 (NDRG1). J Biol Chem. 2012;287(21):17016–28.
101. Mori S, Sawada T, Okada T, Kubota K. Anti-proliferative effect of interferon-gamma is enhanced by iron chelation in colon cancer cell lines in vitro. Hepatogastroenterology. 2008;55(85):1274–9. [PubMed: 18795672]
102. Okada T, Sawada T, Kubota K. Deferoxamine enhances anti-proliferative effect of interferon-gamma against hepatocellular carcinoma cells. Cancer Lett. 2007;248(1):24–31. [PubMed: 16837131]
103. Siriwardana G, Seligman PA. Iron depletion results in Src kinase inhibition with associated cell cycle arrest in neuroblastoma cells. Physiol Rep. 2015;3(3).
104. Kamihara Y, Takada K, Sato T, Kawano Y, Murase K, Arihara Y, et al. The iron chelator deferasirox induces apoptosis by targeting oncogenic Pyk2/beta-catenin signaling in human multiple myeloma. Oncotarget. 2016;7(39):64330–41. [PubMed: 27602957]
105. Woo KJ, Lee TJ, Park JW, Kwon TK. Desferrioxamine, an iron chelator, enhances HIF-1alpha accumulation via cyclooxygenase-2 signaling pathway. Biochem Biophys Res Commun. 2006;343(1):8–14. [PubMed: 16527254]
106. Chen W, Hill H, Christie A, Kim MS, Holloman E, Pavia-Jimenez A, et al. Targeting renal cell carcinoma with a HIF-2 antagonist. Nature. 2016;539(7627):112–7. [PubMed: 27595394]
107. Martinez-Saez O, Gajate Borau P, Alonso-Gordoa T, Molina-Cerrillo J, Grande E. Targeting HIF-2 alpha in clear cell renal cell carcinoma: A promising therapeutic strategy. Critical reviews in oncology/hematology. 2017;111:117–23. [PubMed: 28259286]
108. Cho H, Du X, Rizzi JP, Liberzon E, Chakraborty AA, Gao W, et al. On-target efficacy of a HIF-2alpha antagonist in preclinical kidney cancer models. Nature. 2016;539(7627):107–11. [PubMed: 27595393]
109. Chueh HW, Sung KW, Lee SH, Yoo KH, Koo HH, Kim JY, et al. Iron chelation treatment with deferasirox prior to high-dose chemotherapy and autologous stem cell transplantation may reduce the risk of hepatic veno-occlusive disease in children with high-risk solid tumors. Pediatr Blood Cancer. 2012;58(3):441–7. [PubMed: 21638755]
110. Yu Y, Gutierrez E, Kovacevic Z, Saletta F, Obeidy P, Suryo Rahmanto Y, et al. Iron chelators for the treatment of cancer. Curr Med Chem. 2012;19(17):2689–702. [PubMed: 22455580]

111. Lukmantara AY, Kalinowski DS, Kumar N, Richardson DR. Structure-activity studies of 4-phenyl-substituted 2'-benzoylpyridine thiosemicarbazones with potent and selective anti-tumour activity. Org Biomol Chem. 2013;11(37):6414–25. [PubMed: 23963445]

112. Bergeron RJ, Wiegand J, McManis JS, Bharti N. Desferrithiocin: a search for clinically effective iron chelators. J Med Chem. 2014;57(22):9259–91. [PubMed: 25207964]

113. Ohara T, Tomono Y, Boyi X, Yingfu S, Omori K, Matsukawa A. A novel, nontoxic iron chelator, super-polyphenol, effectively induces apoptosis in human cancer cell lines. Oncotarget. 2018;9(67):32751–60. [PubMed: 30214682]

HIGHLIGHTS

- Free iron levels are elevated in clear cell renal cell carcinoma (ccRCC) cells
- ccRCC cells depend on iron to escape apoptosis and cell cycle arrest
- ccRCC cells depend on iron for HIF-2α protein overexpression and activity
- Clinical iron chelator drugs suppress HIF-2α activity and growth of ccRCC cells
- ccRCC iron dependency is mediated by von Hippel Lindau (*VHL*) gene inactivation

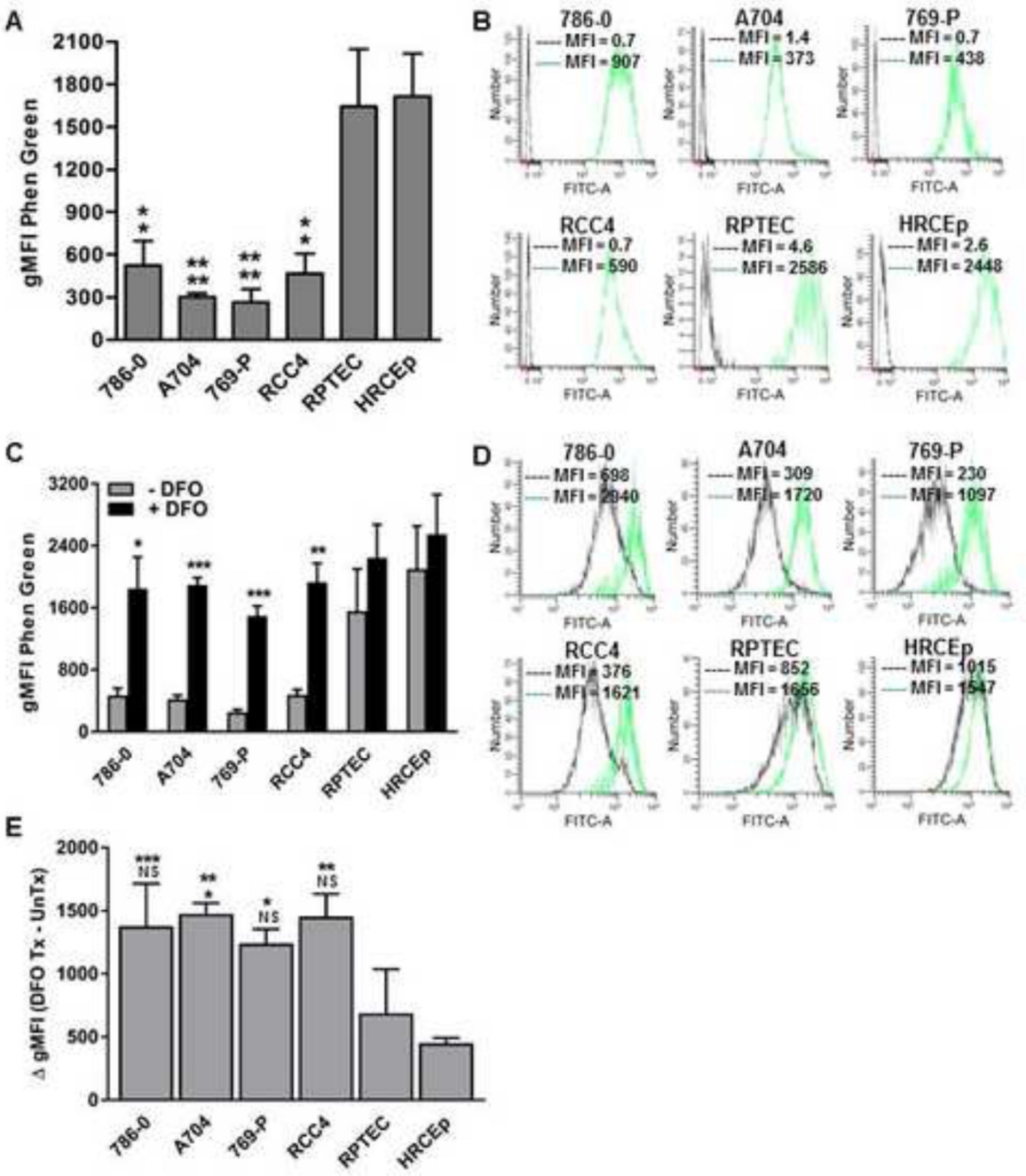

Figure 1. ccRCC cells have increased free iron compared to benign renal cells.

Free iron levels were estimated with Phen Green staining in four ccRCC cell lines (786–0, A704, 769-P, RCC4) and two primary benign human renal epithelial cell lines (RPTEC, HRCEp) at baseline and after prolonged (120-hour) treatment with and without the iron chelator drug, DFO (500 μM). Intracellular free iron level is inversely proportional to the Phen Green geometric mean fluorescence intensity (gMFI) measured using flow cytometry. **(A)** Phen Green mean staining levels (gMFI) in untreated ccRCC and benign renal cell lines. **(B)** Representative flow cytometry histograms of Phen Green stained cells (green)

and unstained cells (black) in untreated ccRCC and benign renal cell lines. **(C)** Phen Green mean staining levels (gMFI) in ccRCC and benign renal cell lines with and without DFO treatment. **(D)** Representative flow cytometry histograms of Phen Green stained ccRCC and benign renal cell lines with (green) or without (black) DFO treatment. **(E)** Differences in gMFI levels of DFO treated versus untreated ccRCC cell lines and benign renal cell lines. All data are compiled from at least 3 independent experiments with error bars denoting SEM; *, $p<0.05$; **, $p<0.01$ and ***, $p<0.001$; NS, non-significant. Data in panel (A) were analyzed by one-way ANOVA with Tukey's post-test, and data in panel (C) were analyzed using two-tailed Student's t-test comparing treated and untreated conditions for each cell line. For panels (A) and (E), the top and bottom asterisk labels denote significance compared to HRCEp and RPTEC, respectively.

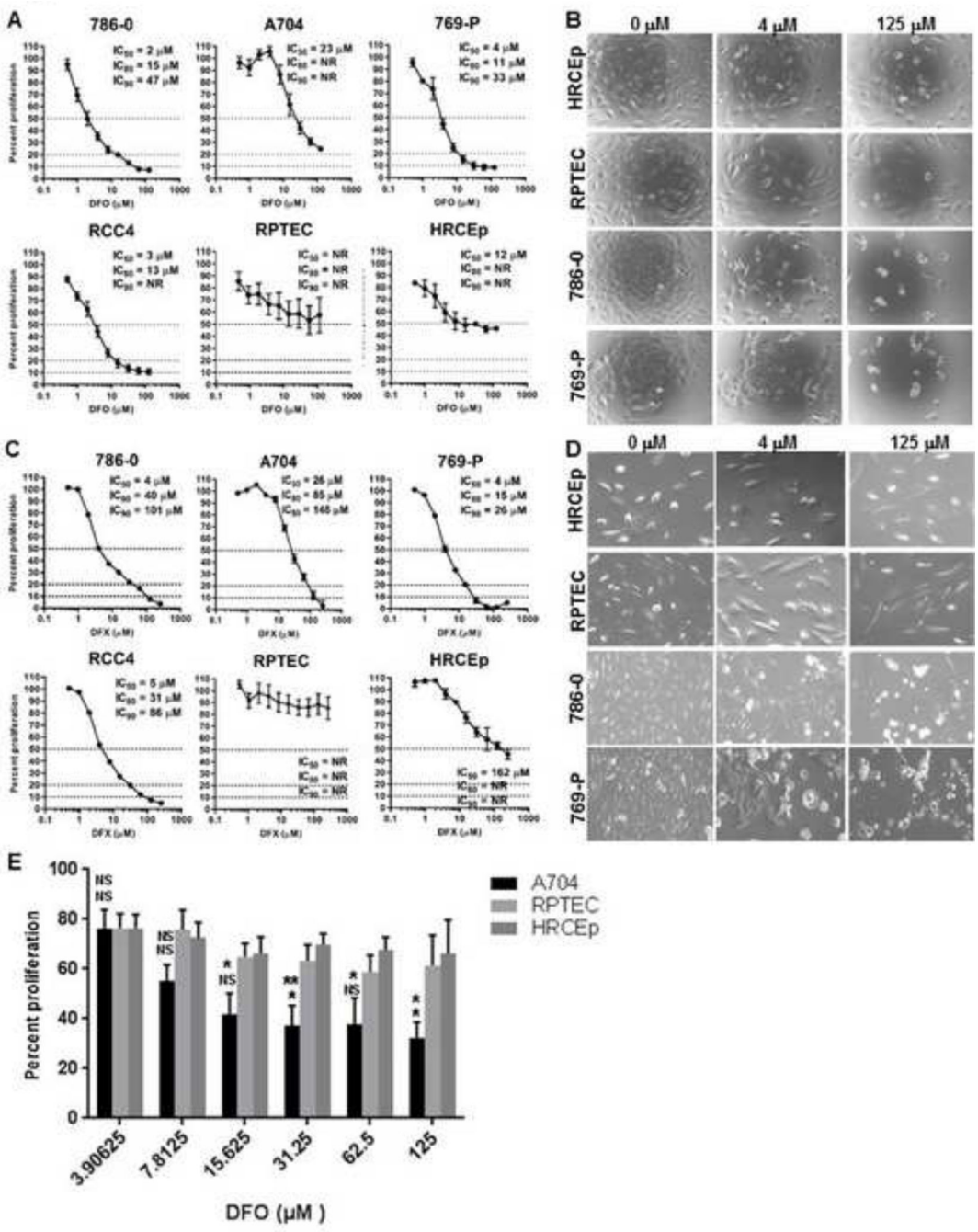

Figure 2. ccRCC cells are more susceptible than benign renal cells to growth suppression with iron chelators.

ccRCC (786–0, A704, 769-P, RCC4) and benign renal epithelial (RPTEC, HRCEp) cell line growth was measured by MTS assay after 72-hour (A-D) and 120-hour (E) treatments with different micromolar concentrations of iron chelating drugs, DFO or DFX. Cell line growth was plotted for each drug concentration as a percentage relative to the untreated cell line growth. **(A)** Growth of DFO-treated cell lines relative to untreated cell lines after 72 hours. **(B)** Representative cell line density and morphology after 72-hour DFO treatment

using light microscopy. **(C)** Growth of DFX-treated cell lines relative to untreated cell lines after 72 hours. **(D)** Representative cell line density and morphology after 72-hour DFO treatment using light microscopy. **(E)** Comparative growth of A704, HRCEp and RPTEC cell lines measured by MTS assay after 120-hour treatment with increasing concentrations of DFO. All data are from at least 3 independent experiments with error bars denoting SEM. Horizontal dashed lines in (A) and (C) represent cut-offs for determining growth IC_{50}, IC_{80} and IC_{90} values. Data in (E) were compared between groups two-tailed Student's t-test and are compiled from three independent experiments. *, $p<0.05$; error bars denote SEM.

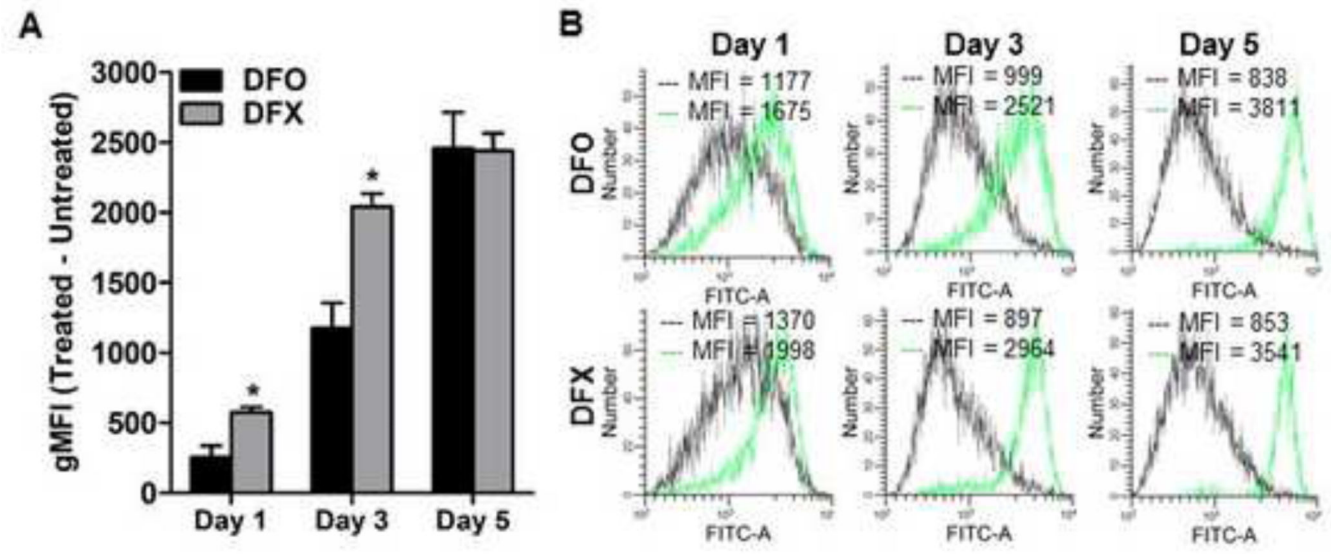

Figure 3. DFX depletes intracellular free iron faster than DFO in A704 cells.

The ccRCC cell line A704 was treated with 125 μM DFO or 125 μM DFX for 1, 3 and 5 days and stained with Phen Green, the fluorescence of which is inversely proportional to the amount of cellular free iron. **(A)** Comparison of A704 free iron levels based on flow cytometry measurement of Phen Green stain after DFO versus DFX treatment relative to untreated cells at different time points. **(B)** Representative flow cytometry histograms of A704 cells with (green) and without (black) DFO or DFX treatment at 1, 3 and 5 days. Data were analyzed using a two-tailed Student's t-test and are compiled from three independent experiments. *, $p<0.05$; error bars denote SEM.

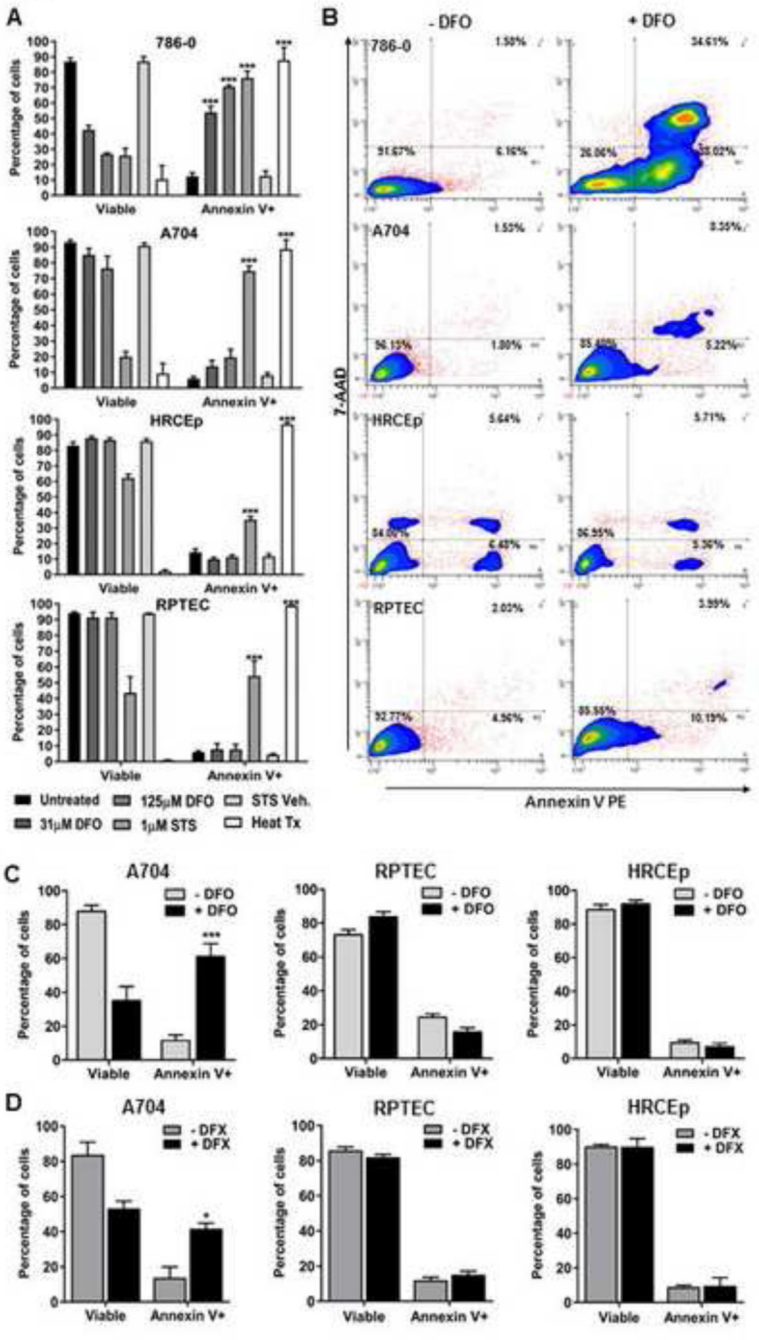

Figure 4. Iron chelation induces apoptosis in ccRCC cell lines but not benign renal cell lines.

Apoptosis was measured using Annexin V and 7AAD stain with flow cytometry in ccRCC (786–0 and A704) and benign renal (RPTEC and HRCEp) cell lines treated with 0, 31 or 125 μM DFO for 48 hours. Staurosporine (STS, 1 μM, 18 hours) drug was used as a positive control for apoptosis induction, in addition to its vehicle control, DMSO (STS Veh.). Heat-treated cells (Heat Tx) were used as a positive control for cell lysis and non-specific cell death. **(A)** Viable (7AAD(−)) and apoptotic (Annexin V(+)) cell percentages for ccRCC and benign renal cell lines are shown after treatment with and without DFO (31 or 125 μM)

or control conditions. **(B)** Representative flow cytometry contour plots for 786–0, A704, HRCEp and RPTEC cells with and without DFO (125 μM) treatment. **(C, D)** Cell lines with resistance to apoptosis induction after 48-hour DFO treatment (A704, HRCEp and RPTEC) were subsequently treated with DFO for 120-hours (C), or DFX for 48 hours (D), and apoptosis was re-measured. All data are compiled from at least 3 independent experiments, with error bars denoting SEM; *, $p<0.05$; **, $p<0.01$ and ***, $p<0.001$ for comparison of treated and untreated cells using a two-tailed Student's t-test.

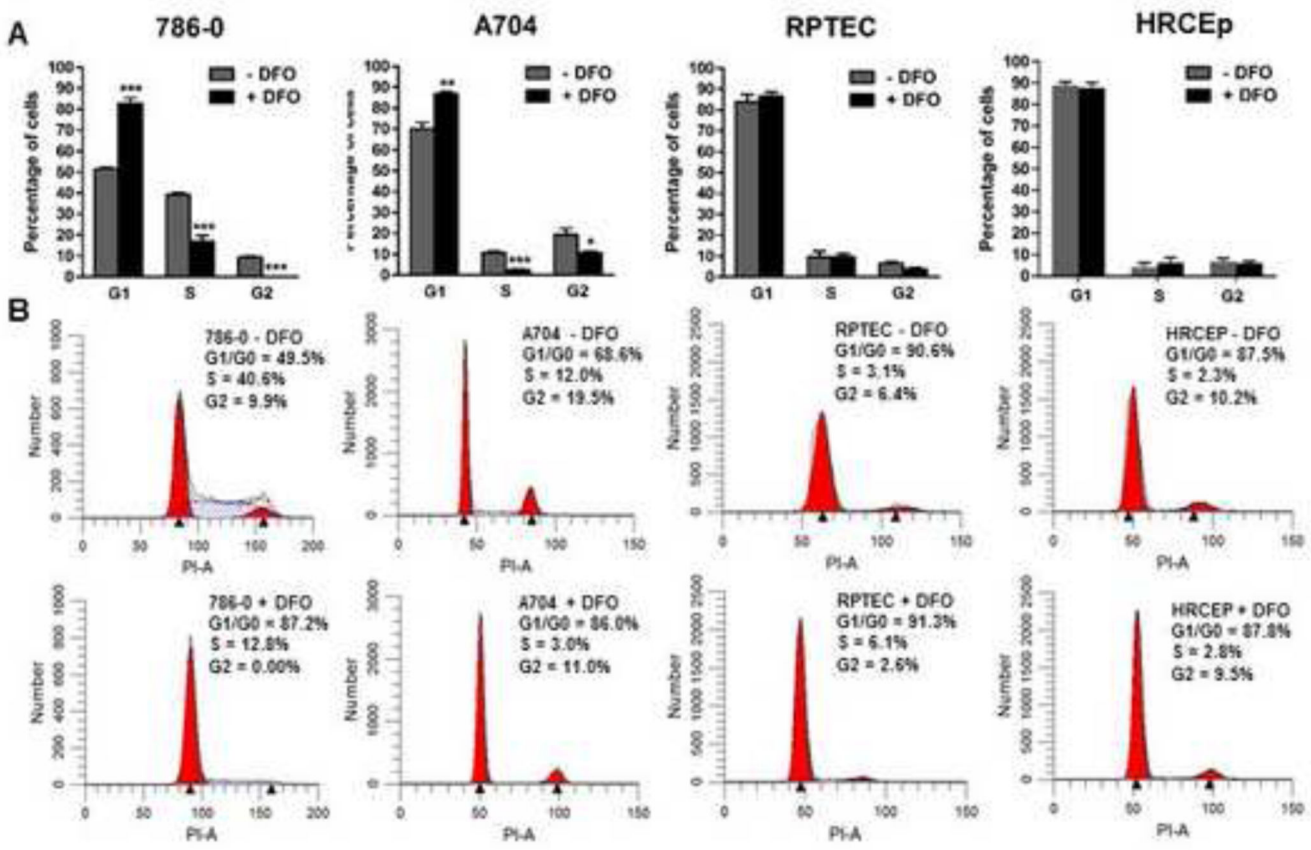

Figure 5. Iron chelation causes G1 cell cycle arrest in ccRCC cells but not benign renal cells.

(A) ccRCC (786–0 and A704) and benign renal (RPTEC and HRCEp) cell lines were treated with 0 or 125 μM DFO for 48 hours and percentage of cells in different cell cycle phases were analyzed by flow cytometry after staining with propidium iodide. **(B)** Representative flow cytometry histograms from cell cycle analyses of DFO-treated and untreated cells. Data are compiled from at least 3 independent experiments, with error bars denoting SEM; *, $p<0.05$ and ***, $p<0.001$ for comparisons of treated and untreated cells at each cell cycle phase using a two-tailed Student's t-test.

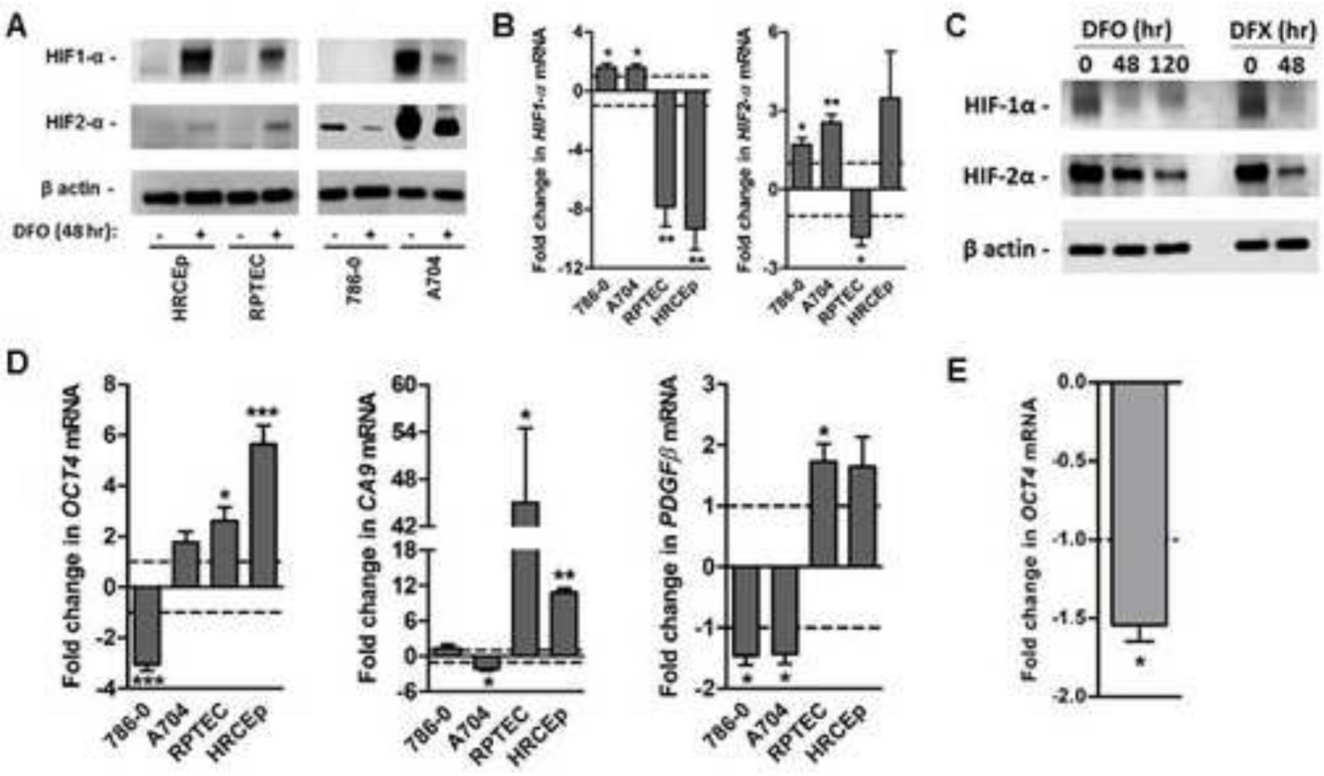

Figure 6. Iron deprivation suppresses HIF-α protein levels and transcriptional activity in ccRCC cells but not benign renal cells.

ccRCC (786–0 and A704) and benign renal (RPTEC and HRCEp) cell lines were treated with and without 125 μM DFO for 48 hours (all cell lines) and 120 hours (A704 only), or with 125 μM DFX for 48 hours (A704 only). Treated cells were analyzed using Western blot to measure HIF1-α and HIF2-α protein levels, with β actin protein as a loading control; and using quantitative PCR (qPCR) to measure mRNA transcript levels of HIF-α transcriptional targets (*CA9, OCT4, PDFGβ*). **(A)** Representative Western blot of HIF-1α and HIF-2α proteins in ccRCC and benign renal cell lines with and without 48-hour DFO treatment. **(B)** Changes in gene expression for *HIF-1α* and *HIF-2α/EPAS1* with and without 48-hour DFO treatment. **(C)** Representative western blots of HIF-2α protein levels in A704 cells treated with DFO for 0, 48 and 120 hours (left panel), or with and without DFO or DFX for 48 hours (right panel). **(D)** Changes in expression of HIF-α transcriptional target genes, *CA9* (HIF1α), *OCT4* (HIF-2α) and *PDGF-β* (HIF-1α/HIF-2α) after 48-hour DFO treatment. **(E)** Changes in *OCT4* gene expression in A704 cells after extended (120-hour) DFO treatment. For gene expression data, mean levels in treated cells are normalized to those of untreated cells (dashed line). All data are from at least 3 independent experiments, with error bars denoting SEM. *, $p<0.05$; **, $p<0.01$ and ***, $p<0.001$ for comparison of treated and untreated cells using a one-sample t-test.

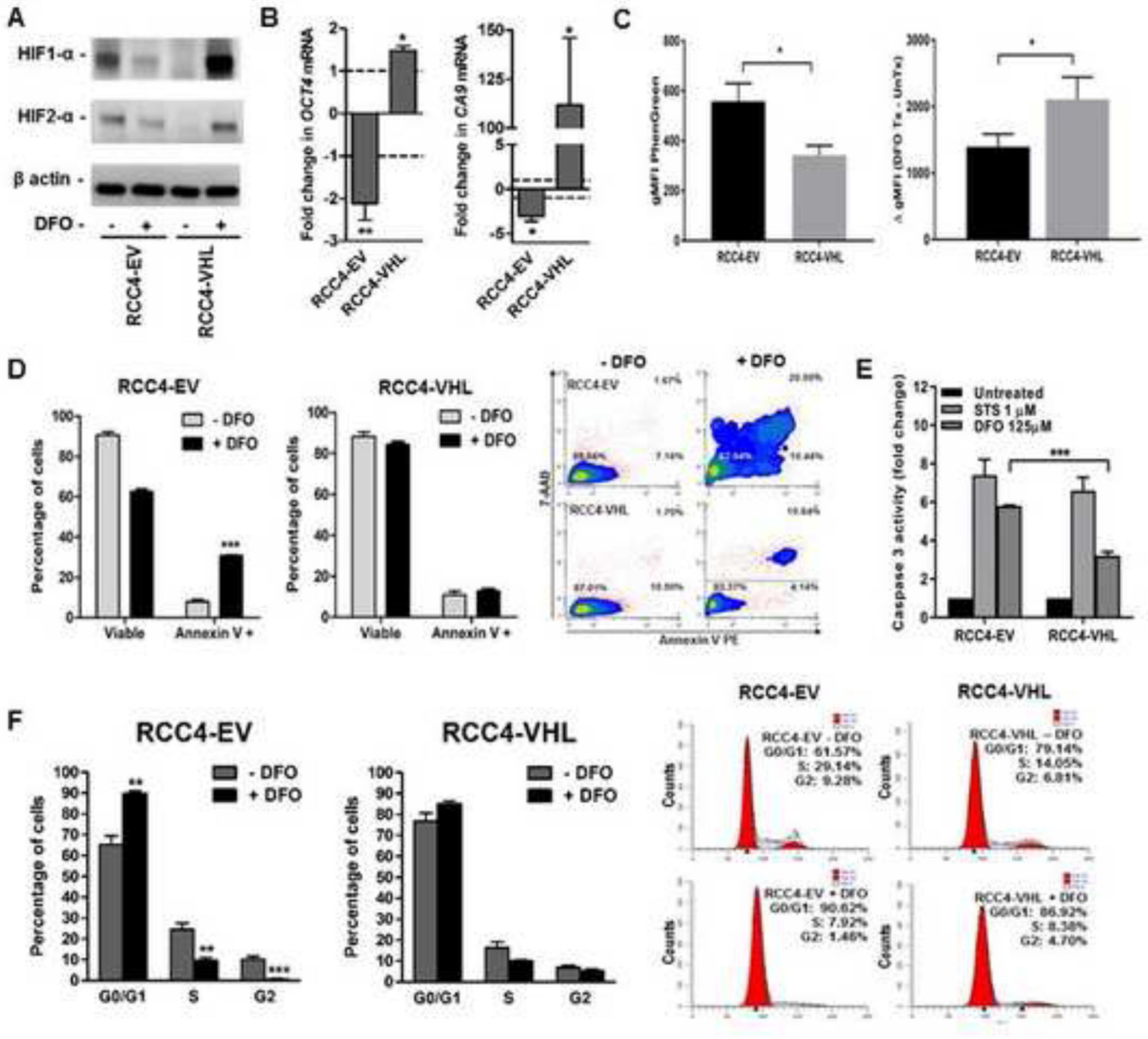

Figure 7. Iron chelation-induced apoptosis and cell cycle arrest in ccRCC cells is dependent on VHL loss.

RCC4-EV and RCC4-VHL cell lines were treated with 125 μM DFO for 48 or 120 hours and compared for levels of free iron, HIF-α protein, HIF-α target gene expression, apoptosis and cell cycle arrest. **(A)** Representative Western blot of HIF-1α and HIF-2α protein with β actin as a loading control in RCC4-EV and RCC4-VHL cell lines following 48-hour DFO treatment. **(B)** Changes in *CA9* (HIF-1α target) and *OCT4* (HIF-2α target) gene expression in RCC4-EV and RCC4-VHL cell lines following 48-hour DFO treatment, as measured using qRT-PCR. Mean changes in treated cells are normalized to those of untreated cells (dashed line). **(C)** Free iron levels in RCC4-EV and RCC4-VHL cell lines, as determined using flow cytometry measurement of Phen Green stain geometric mean fluorescence intensity (gMFI), which is inversely proportional to cellular free iron levels.

(D) Cell viability and apoptosis based on staining with 7-AAD and Annexin V, respectively, in RCC4-EV and RCC4-VHL cells treated with and without DFO for 48 hours, as measured using flow cytometry. **(E)** Representative flow cytometry contour plots of Annexin V/7-AAD staining in untreated and DFO-treated RCC4-EV and RCC4-VHL cells. **(F)** Caspase 3 activity following 48-hour treatment with DFO in RCC4-EV and RCC4-VHL cells. **(G)** Cell cycle phase analysis using flow cytometry measurement of propidium iodide stain after DFO treatment in RCC4-EV and RCC4-VHL cells. All data are from at least 3 independent experiments, with error bars denoting SEM; *, $p<0.05$; **, $p<0.01$ and ***, $p<0.001$ for comparison of RCC4-EV vs. RCC4-VHL (C and F) or treated vs. untreated cells (B, D, F) using a two-tailed Student's t-test (C, D, F), one-sample t-test (B) or a one-way ANOVA with Tukey's post-test (E).